

Quasinormal-mode spectrum of Kerr black holes and its geometric interpretation

Huan Yang,¹ David A. Nichols,¹ Fan Zhang,¹ Aaron Zimmerman,¹ Zhongyang Zhang,² and Yanbei Chen¹

¹*Theoretical Astrophysics 350-17, California Institute of Technology, Pasadena, CA 91125, USA*

²*Department of Physics and Astronomy, The University of Mississippi, University, MS 38677, USA*

There is a well-known, intuitive geometric correspondence between high-frequency quasinormal modes of Schwarzschild black holes and null geodesics that reside on the light-ring (often called spherical photon orbits): the real part of the mode's frequency relates to the geodesic's orbital frequency, and the imaginary part of the frequency corresponds to the Lyapunov exponent of the orbit. For slowly rotating black holes, the quasinormal-mode's real frequency is a linear combination of the orbit's precessional and orbital frequencies, but the correspondence is otherwise unchanged. In this paper, we find a relationship between the quasinormal-mode frequencies of Kerr black holes of arbitrary (astrophysical) spins and general spherical photon orbits, which is analogous to the relationship for slowly rotating holes. To derive this result, we first use the WKB approximation to compute accurate algebraic expressions for large- l quasinormal-mode frequencies. Comparing our WKB calculation to the leading-order, geometric-optics approximation to scalar-wave propagation in the Kerr spacetime, we then draw a correspondence between the real parts of the parameters of a quasinormal mode and the conserved quantities of spherical photon orbits. At next-to-leading order in this comparison, we relate the imaginary parts of the quasinormal-mode parameters to coefficients that modify the amplitude of the scalar wave. With this correspondence, we find a geometric interpretation to two features of the quasinormal-mode spectrum of Kerr black holes: First, for Kerr holes rotating near the maximal rate, a large number of modes have nearly zero damping; we connect this characteristic to the fact that a large number of spherical photon orbits approach the horizon in this limit. Second, for black holes of any spins, the frequencies of specific sets of modes are degenerate; we find that this feature arises when the spherical photon orbits corresponding to these modes form closed (as opposed to ergodically winding) curves.

PACS numbers: 04.25.-g, 04.30.Nk, 4.70.Bw

I. INTRODUCTION

Quasinormal modes (QNMs) of black-hole spacetimes are the characteristic modes of linear perturbations of black holes that satisfy an outgoing boundary condition at infinity and an ingoing boundary condition at the horizon (they are the natural, resonant modes of black-hole perturbations). These oscillatory and decaying modes are represented by complex characteristic frequencies $\omega = \omega_R - i\omega_I$, which are typically indexed by three numbers, n , l , and m . The overtone number n is proportional to the decay rate of the perturbation, and l and m are multipolar indexes of the angular eigenfunctions of the QNM.

A. Overview of quasinormal modes and their geometric interpretation

Since their discovery, numerically, in the scattering of gravitational waves in the Schwarzschild spacetime by Vishveshwara [1], QNMs have been thoroughly studied in a wide range of spacetimes, and they have found many applications. There are several reviews [2–6] that summarize the many discoveries about QNMs. They describe how QNMs are defined, the many methods used to calculate QNMs (e.g., estimating them from time-domain solutions [7], using shooting methods in frequency-domain calculations [8], approximating them with inverse-potential approaches [9] and WKB methods [10, 11], and numerically solving for them with continued-fraction techniques [12, 13]), and the ways to quantify the excitation of QNMs (see, e.g., [14, 15]). They also discuss the prospects

for detecting them in gravitational waves using interferometric gravitational-wave detectors, such as LIGO [16] and VIRGO [17], and for inferring astrophysical information from them (see, e.g., [18, 19] for finding the mass and spin of black holes using QNMs, [20, 21] for quantifying the excitation of QNMs in numerical-relativity simulations binary-black-hole mergers, and [22, 23] for testing the no-hair theorem with QNMs). There have also been several other recent applications of QNMs. For example, Zimmerman and Chen [24] (based on work by Mino and Brink [25]) study extensions to the usual spectrum of modes generated in generic ringdowns. Dolan and Ottewill use eikonal methods to approximate the modal wave function, and they use these functions to study the Green's function and to help understand wave propagation in the Schwarzschild spacetime [26–28].

Although QNMs are well-understood and can be calculated quite precisely, it remains useful to develop intuitive and analytical descriptions of these modes. An important calculation in this direction was performed by Ferrari and Mashhoon [9], who showed that for a Schwarzschild black hole, the QNM frequency (which depends only on a multipolar index l and an overtone index n) can be written in the eikonal (or geometric-optics) limit, $l \gg 1$, as

$$\omega \approx (l + 1/2)\Omega - i\gamma_L(n + 1/2). \quad (1.1)$$

The quantities Ω and γ_L are, respectively, the Keplerian frequency of the circular photon orbit and the Lyapunov exponent of the orbit, the latter of which characterizes how quickly a congruence of null geodesics on the circular photon orbit increases its cross section under infinitesimal radial perturbations [28, 29]. Equation (1.1) hints at an intriguing physical description of QNMs: for modes with wavelengths much

shorter than the background curvature, the mode behaves as if it were sourced by a perturbation that orbits on and diffuses away from the light ring on the time scale of the Lyapunov exponent.

Ferrari and Mashhoon [9] also derived an analogous result to Eq. (1.1) for slowly rotating black holes. They showed for $l \gtrsim m \gg 1$, the real part of the frequency is given by

$$\Omega \approx \omega_{\text{orb}} + \frac{m}{l+1/2} \omega_{\text{prec}}, \quad (1.2)$$

where ω_{orb} is now the Keplerian orbital frequency for the circular photon orbit and ω_{prec} is the Lense-Thirring-precession frequency of the orbit (which arises because of the slow rotation of the black hole). The term proportional to ω_{prec} also has a simple geometric-optics interpretation. Inertial frames near the high-frequency wave at the light ring are dragged with respect to inertial frames at infinity, and this frame dragging causes the perturbation's orbit to precess about the spin axis of the black hole with a frequency, ω_{prec} . If the orbit is inclined at an angle of $\sin^2 \theta = m^2/l(l+1)$ (the ratio of angular momenta L_z^2/L^2 for quantized waves in flat space), then the projection of the precessional velocity onto the orbital plane scales the precessional frequency by a factor of $\sim m/(l+1/2)$.

Why the QNM frequency is multiplied by $(l+1/2)$ is a feature that we will explain in greater detail in this paper. Intuitively, this term arises because in the high-frequency limit, any wavefront traveling on null orbits will have an integral number of oscillations in the θ and ϕ directions. For the wave to be periodic and single-valued, there must be m oscillations in the ϕ direction. For the θ direction, it is a Bohr-Sommerfeld quantization condition that requires $l - |m| + 1/2$ oscillations in this direction, which implies that there should be a net spatial frequency of roughly $(l+1/2)$. This increases the frequency of the radiation seen far from the hole by the same factor.

From this intuitive argument, we expect that the real part of the mode should be

$$\omega_R = L \left(\omega_{\text{orb}} + \frac{m}{L} \omega_{\text{prec}} \right), \quad (1.3)$$

where we define $L = l + 1/2$. In this paper, we will show that an equation of the form of Eq. (1.3) does, in fact, describe the QNM frequencies of Kerr black holes of arbitrary astrophysical spins (and it recovers the result of Ferrari and Mashhoon for slowly spinning black holes). As we mention in the next part of this section, the exact details of the correspondence between QNMs and photon orbits is richer for rapidly rotating black holes than for slowly rotating or static black holes.

B. Methods and results of this article

To derive Eq. (1.3) requires that we develop a geometric-optics interpretation of the QNMs of Kerr black holes with arbitrary astrophysical spins. Finding the correspondence requires two steps: first, we need to calculate the approximate frequencies using the WKB method; next, we must articulate a connection between the mathematics of waves propagating

in the Kerr spacetime in the geometric-optics approximation and those of the WKB approximation (the first step). Finally, with the geometric-optics description of QNMs, we can make a physical interpretation of the spectrum (for example, the degeneracy or the lack of damping in the extremal limit).

In Sec. II, we describe how we solve the eigenvalue problem that arises from separating the Teukolsky equation [30] (a linear partial differential equation that describes the evolution of scalar, vector, and gravitational perturbations of Kerr black holes) into two nontrivial linear ordinary differential equations. The two differential equations, the radial and angular Teukolsky equations, share two unknown constants—the frequency, ω , and the angular separation constant, A_{lm} —that are fixed by the boundary conditions that the ordinary differential equations must satisfy (ingoing at the horizon and outgoing at infinity for the radial equation, and well-behaved at the poles for the angular equation). The goal of the WKB method is to compute the frequency and separation constant approximately.

Although there has been work by Kokkotas [31] and Iyer and Seidel [32] using WKB methods to compute QNM frequencies of rotating black holes, their results were limited to slowly rotating black holes, because they performed an expansion of the angular separation constant, A_{lm} , for small, dimensionless spin parameters, a/M , and only applied the WKB method to the radial Teukolsky equation to solve for the frequency. In a different approach, Dolan developed a matched-expansion formalism for Kerr black holes of arbitrary spins that can be applied to compute the frequency of QNMs, but only for modes with $l = |m|$ and $m = 0$ [27].

Therefore, it remains an outstanding problem to compute a WKB approximation to the quasinormal modes of Kerr black holes of large spins and for any multipolar index m . In Sec. II, we solve the joint eigenvalue problem of the radial and angular Teukolsky equations by applying a change of variables to the angular equation that brings it into the form of a bound-state problem in quantum mechanics. Applying the WKB method to the angular equation, we arrive at a Bohr-Sommerfeld condition that constrains the angular constant in terms of the frequency (and the indices l and m). Simultaneously, we can analyze the radial equation in the WKB approximation, and the two equations together define a system of integral equations, which can be solved for the eigenvalues. When we expand the Bohr-Sommerfeld condition in a Taylor series in terms of the numerically small parameter, $a\omega/l$, the system of integral equations reduces to an algebraic system (which, in turn, leads to a simpler expression for the frequency). The approximate frequency agrees very well with the result that includes all powers of $a\omega/l$, and, in the eikonal limit, it is accurate to order $1/l$ for Kerr black holes of arbitrary spins, for modes with any value of m , and for both the real and the imaginary parts of the frequency.

To interpret the WKB calculation of Sec. II in the language of propagating waves in the geometric-optics limit within the Kerr spacetime, we analyze waves around a Kerr black hole in Sec. III using the geometric-optics approximation and the Hamilton-Jacobi formalism. We confirm that the leading-order pieces of the WKB frequencies and angu-

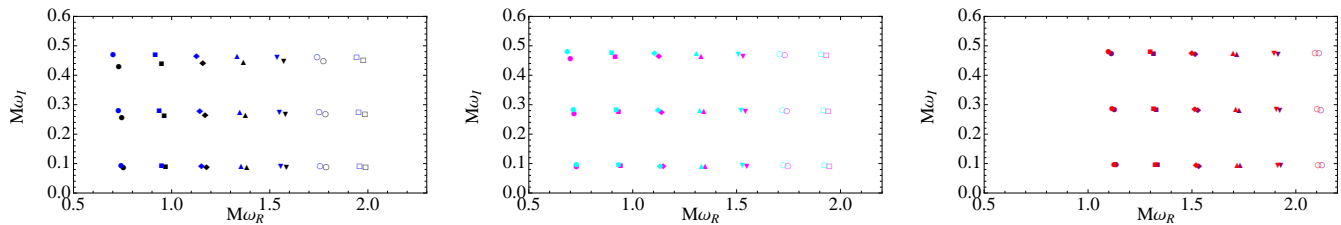


Figure 1: Low-overtone QNM spectrum of three Kerr black holes of different spins with approximate degeneracies in their spectra. From left to right, we plot the three lowest-overtone QNM excitations for (i) $a/M = 0.69$ in which $(l, m) = (j, 2)$ are black symbols and $(l', m') = (j+1, -2)$ are blue symbols, where $j = 3, \dots, 9$; (ii) $a/M = 0.47$ in which $(l, m) = (j, 3)$ are magenta symbols and $(l', m') = (j+1, -3)$ are cyan symbols, where $j = 3, \dots, 9$; (iii) $a/M = 0.35$ in which $(l, m) = (j, 4)$ are red symbols and $(l', m') = (j+1, -4)$ are purple symbols, where $j = 5, \dots, 10$. For these spin parameters, the mode with positive values of m and ω_R (a corotating mode) of index l is approximately degenerate with the mode with $m' = -m$, and ω_R (a counterrotating mode) of index $l' = l+1$.

lar constants correspond to the conserved quantities of the leading-order, geodesic behavior of the geometric-optics approximation (specifically, the real part of ω , the index m , and the real part of A_{lm} are equivalent to the energy \mathcal{E} , the z -component of the specific angular momentum L_z , and Carter's constant \mathcal{Q} plus L_z^2 , respectively). The specific geodesics corresponding to a QNM are, in fact, spherical photon orbits. The next-to-leading-order WKB quantities (the imaginary parts of ω and A_{lm}) correspond to dispersive, wavelike corrections to the geodesic motion (they are the Lyapunov exponent and the product of this exponent with the change in Carter's constant with respect to the energy). Table I in Sec. III summarizes this geometric-optics correspondence.

In Sec. IV, we make several observations about features of the QNM spectrum of Kerr black holes that have simple geometric interpretations. First, we find that for extremal Kerr black holes, a significant fraction of the QNMs have a real frequency proportional to the angular frequency of the horizon and a decay rate that rapidly falls to zero; we explain this in terms of a large number of spherical photon orbits that collect on the horizon for extremal Kerr holes. Second, we expand the WKB expression for the real part of the frequency as in Eq. (1.3), and we interpret these terms as an orbital and a precessional frequency of the corresponding spherical photon orbit. These two frequencies depend on the spin of the black hole and the value of m/L very weakly for slowly-rotating black holes, though quite strongly when the spin of the black hole is nearly extremal. Finally, we use the geometric-optics interpretation given by Eq. (1.3) to explain a degeneracy in the QNM spectrum of Kerr black holes, in the eikonal limit, which also manifests itself, approximately, for small l (see Fig. 1). The degeneracy occurs when the orbital and precession frequencies, ω_{orb} and ω_{prec} are rationally related (i.e., $\omega_{\text{orb}}/\omega_{\text{prec}} = p/q$ for integers p and q) for a hole of a specific spin parameter, and when the corresponding spherical photon orbits close. By substituting this result into Eq. (1.3) one can easily see that modes with multipolar indexes l and m become degenerate with those of indexes $l' = l+kq$ and $m' = m-kp$ for any non-negative integer k , in the eikonal limit (note that in Fig. 1, we show an approximate degeneracy for $k=1$ and for three spin parameters, such that $q/p = 1/4, 1/6, \text{ and } 1/8$,

respectively.)

To conclude this introduction, we briefly summarize the organization of this paper: In Sec. II, we review the Teukolsky equations, and we then describe the WKB formalism that we use to calculate an accurate approximation to the angular eigenvalues $A_{lm} = A_{lm}^R + iA_{lm}^I$ and QNM frequencies $\omega = \omega_R - i\omega_I$, in the eikonal limit $L \gg 1$ and for holes of arbitrary spins. We verify the accuracy of our expressions in Sec. IID by comparing the WKB frequencies to exact, numerically calculated frequencies. In Sec. III, we develop a correspondence between the WKB calculation and mathematics of wave propagation within the Kerr spacetime in the geometric-optics limit, using the geometric-optics approximation and the Hamilton-Jacobi formalism. At leading-order, the QNM frequencies and angular eigenvalues correspond to the conserved quantities of motion in the Kerr spacetime for spherical photon orbits; at next-to-leading order in the geometric-optics approximation, we connect the decaying behavior of the QNMs to dispersive behaviors of the waves. Finally, in Sec. IV, we interpret aspects of the QNM spectrum geometrically, such as the vanishing of the damping rate for many modes of extremal black holes, the decomposition of the frequency into orbital and precessional parts, and the degeneracies in the QNM frequency spectrum. Finally, in Sec. V, we conclude. We use geometrized units in which $G = c = 1$ and the Einstein summation convention throughout this paper.

II. WKB APPROXIMATION FOR THE QUASINORMAL-MODE SPECTRUM OF KERR BLACK HOLES

In this section, we will derive expressions for the frequencies of quasinormal modes of Kerr black holes using the WKB approximation. We will need to compute the real and imaginary parts to an accuracy of $O(1)$ in terms of $l \gg 1$, which implies that we must calculate ω_R to leading and next-to-leading order and ω_I to leading order. Here, we will focus on obtaining an analytic approximation to the frequency spectrum, and we will leave the geometrical interpretation of our results until the next section.

Before specializing our results to the angular and radial Teukolsky equations, we will review a basic result about the WKB expansion that we will use frequently throughout this paper; a more complete discussion of WKB methods can be found in [11]. Given a wave equation for $\psi(x)$

$$\varepsilon^2 \frac{d^2 \psi}{dx^2} + U(x) \psi = 0, \quad (2.1)$$

we will expand the solution as $\psi = e^{S_0/\varepsilon + S_1 + \varepsilon S_2 + \dots}$, where the leading and next-to-leading action variables are given by

$$S_0 = \pm i \int^x \sqrt{U(x)} dx, \quad (2.2a)$$

$$S_1 = -\frac{1}{4} \log U(x). \quad (2.2b)$$

The formulas above will be the basis for our analysis of the radial and angular Teukolsky equations in the next sections.

A. The Teukolsky equations

Teukolsky showed that scalar, vector, and tensor perturbations of the Kerr spacetime all satisfy a single master equation for scalar variables of spin weight s ; moreover, the master equation can be solved by separation of variables [30]. We will use u to denote our scalar variable, and we will separate this scalar wave as

$$u(t, r, \theta, \phi) = e^{-i\omega t} e^{im\phi} u_r(r) u_\theta(\theta). \quad (2.3)$$

Then, at the relevant order in $l \gg 1$, the angular equation for $u_\theta(\theta)$ can be written as

$$\frac{1}{\sin \theta} \frac{d}{d\theta} \left[\sin \theta \frac{du_\theta}{d\theta} \right] + \left[a^2 \omega^2 \cos^2 \theta - \frac{m^2}{\sin^2 \theta} + A_{lm} \right] u_\theta = 0, \quad (2.4)$$

where A_{lm} is the angular eigenvalue of this equation. The equation obeyed by the radial function $u_r(r)$ is

$$\frac{d^2 u_r}{dr_*^2} + \frac{K^2 - \Delta \lambda_{lm}^0}{(r^2 + a^2)^2} u_r = 0, \quad \frac{d}{dr_*} \equiv \frac{\Delta}{r^2 + a^2} \frac{d}{dr} \quad (2.5a)$$

with

$$K = -\omega(r^2 + a^2) + am, \quad (2.5b)$$

$$\lambda_{lm}^0 = A_{lm} + a^2 \omega^2 - 2am\omega, \quad (2.5c)$$

$$\Delta = r^2 - 2Mr + a^2. \quad (2.5d)$$

Here we have used the facts that $\omega_R \sim O(l)$, $\omega_I \sim O(1)$, $m \sim O(l)$ to drop terms that are of higher orders in the expansion than those that we treat. Note that the spin s of the perturbation no longer enters into these equations after neglecting the higher-order terms.

B. The angular eigenvalue problem

We will first find an expression for A_{lm} in terms of ω , l , and m , by analyzing the angular equation in the WKB approximation. By defining

$$x = \log \left(\tan \frac{\theta}{2} \right) \quad (2.6)$$

and $dx = d\theta / \sin \theta$, we can write the angular equation as

$$\frac{d^2 u_\theta}{dx^2} + V^\theta u_\theta = 0, \quad (2.7a)$$

where

$$V^\theta = a^2 \omega^2 \cos^2 \theta \sin^2 \theta - m^2 + A_{lm} \sin^2 \theta. \quad (2.7b)$$

When written in this form, it is clear that u_θ must satisfy a boundary condition that it be 0 as $x \rightarrow \pm\infty$ (which corresponds to $\theta \rightarrow 0, \pi$). Furthermore, the angular equation is now in a form that is amenable to a WKB analysis (which will be the subject of the next part).

First, however, we outline how we will perform the calculation. Because the frequency $\omega = \omega_R - i\omega_I$ is complex, the angular eigenvalue A_{lm} , a function of ω , must also be complex. We will write

$$A_{lm} = A_{lm}^R + iA_{lm}^I, \quad (2.8)$$

to indicate the split between real and imaginary parts. We will treat a real-valued $\omega = \omega_R$ in the first part of this section, and, therefore, a real-valued $A_{lm}^R(\omega_R)$; we shall account for $-i\omega_I$ by including it as an additional perturbation in the next part of this section.

1. Real part of A_{lm} for a real-valued ω

For $\omega_R \in \mathbb{R}$, we will compute the eigenvalues $A_{lm}^R(\omega_R)$, of Eq. (2.7a) for standing-wave solutions that satisfy physical boundary conditions. At the boundary, $\theta = 0, \pi$ (or $x = \mp\infty$) the potential satisfies $V^\theta = -m^2$ independent of the value of A_{lm}^R ; this implies that the solutions to Eq. (2.7a) behave like decaying exponential functions at these points (i.e., the wave does not propagate). For there to be a region where the solutions oscillate (i.e., where the wave would propagate), A_{lm} must be sufficiently large to make $V^\theta > 0$ in some region. Depending on the relative amplitudes of A_{lm} and $a^2 \omega^2$, V^θ either has one maximum at $\theta = \pi/2$ (when $A_{lm} \geq a^2 \omega^2$), or two identical maxima at two locations at symmetrically situated around $\theta = \pi/2$ (when $A_{lm} < a^2 \omega^2$). It turns out that the region where the maximum of $V^\theta > m^2$ is centered around $\pi/2$; therefore, all solutions fall into the former category rather than the latter.

The length scale over which the function u_θ varies is $1/\sqrt{V^\theta}$, and the WKB approximation is valid only if the potential V^θ does not vary much at this scale. Therefore, to use the WKB approximation, we require that

$$\left| \frac{1}{\sqrt{V^\theta}} \frac{dV^\theta}{d\theta} \right| \ll |V^\theta|. \quad (2.9)$$

This condition applies regardless of the sign of V^θ . Empirically, we find this condition to hold for V^θ in Eq. (2.7a), except around points at which $V^\theta = 0$. We will refer to these as *turning points*, and they can be found by solving for the zeros of the potential,

$$a^2 \omega_R^2 \cos^2 \theta_\pm \sin^2 \theta_\pm - m^2 + A_{lm}^R \sin^2 \theta_\pm = 0, \quad (2.10)$$

which are given by

$$\sin^2 \theta_\pm = \frac{2m^2}{A_{lm} + a^2 \omega_{lm}^2 \mp \sqrt{(A_{lm} + a^2 \omega_{lm}^2)^2 + 4m^2}}. \quad (2.11)$$

Using the leading and next-to-leading WKB approximation, we can write the solution to the wave equation in the propagative region, $x_- < x < x_+$, as

$$u_\theta(x) = \frac{a_+ e^{i \int_0^x dx' \sqrt{V^\theta(x')}} + a_- e^{-i \int_0^x dx' \sqrt{V^\theta(x')}}}{[V^\theta(x)]^{1/4}}, \quad (2.12)$$

where a_\pm are constants that must be fixed by the boundary conditions that the solution approach zero at $\theta = 0, \pi$. For $x > x_+$, we find

$$u_\theta(x) = \frac{c_+ e^{-\int_{x_+}^x dx' \sqrt{-V^\theta(x')}}}{[V^\theta(x)]^{1/4}}, \quad (2.13a)$$

and $x < x_-$,

$$u_\theta(x) = \frac{c_- e^{-\int_x^{x_-} dx' \sqrt{-V^\theta(x')}}}{[V^\theta(x)]^{1/4}}, \quad (2.13b)$$

with c_\pm also being constants set by the boundary conditions. Note that outside of the turning points, we have only allowed the solution that decays towards $x \rightarrow \pm\infty$.

Around the turning points x_\pm , the WKB approximation breaks down, but u_θ can be solved separately by using the fact that $V_\theta(x \sim x_\pm) \propto x - x_\pm$. Solutions obtained in these regions can be matched to Eqs. (2.12)–(2.13b); the matching condition leads to the Bohr-Sommerfeld quantization condition

$$\int_{\theta_-}^{\theta_+} d\theta \sqrt{a^2 \omega_R^2 \cos^2 \theta - \frac{m^2}{\sin^2 \theta} + A_{lm}^R} = (L - |m|) \pi. \quad (2.14)$$

Here we have defined

$$L \equiv l + \frac{1}{2}, \quad (2.15)$$

which will be used frequently throughout this paper. The limits of the integration are the values of θ where the integrand vanishes [the turning points of Eq. (2.11)].

If we define

$$\mu \equiv \frac{m}{L}, \quad \alpha_R(a, \mu) \equiv \frac{A_{lm}^R}{L^2}, \quad \Omega_R(a, \mu) \equiv \frac{\omega_R}{L}, \quad (2.16)$$

then all three of these quantities are $O(1)$ in our expansion in L . From these definitions, we can re-express the limits of integration as

$$\sin^2 \theta_\pm = \frac{2\mu^2}{\alpha + a^2 \Omega^2 \mp \sqrt{(\alpha + a^2 \Omega_R^2)^2 + 4\mu^2}}, \quad (2.17)$$

and the integral as

$$\int_{\theta_-}^{\theta_+} d\theta \sqrt{\alpha_R - \frac{\mu^2}{\sin^2 \theta} + a^2 \Omega^2 \cos^2 \theta} = (1 - |\mu|) \pi. \quad (2.18)$$

For each set of quantities $(\alpha_R, \mu, \Omega_R)$, we can express α_R as an implicit function involving elliptic integrals; however, if we treat $a\Omega_R$ as a small parameter, then the first two terms in the expansion are

$$\alpha_R \approx 1 - \frac{a^2 \Omega_R^2}{2} (1 - |\mu|^2). \quad (2.19)$$

We derive and discuss this approximation in greater detail in Appendix A. For $a = 0$, we note that this is accurate with a relative error of $O(1/L^2)$, because for a Schwarzschild black hole

$$A_{lm}^{\text{Schw}} = l(l+1) - s(s+1). \quad (2.20)$$

As we will confirm later in Figs. 2 and 4, Eq. (2.19) is an excellent approximation even for highly spinning black holes.

To understand intuitively why the approximation works so well, we will focus on corotating modes (i.e., those with positive and large m , or μ near unity), which have the highest frequencies and, therefore, the largest possible values for $a\Omega_R$. For a fixed value of (l, m) , ω_R is a monotonically increasing function of a , and

$$\omega_R^{lm}(a) \leq \omega_R^{lm}(a = M) = m \Omega_H^{a=1} = \frac{m}{2M}. \quad (2.21)$$

In setting this upper bound, we have used the result that the low-overtone QNM frequencies approach $m\Omega_H$ for $m > 0$ and for extremal black holes (first discussed by Detweiler [33]); we have also used Ω_H to denote the horizon frequency of the Kerr black hole,

$$\Omega_H = \frac{a}{2Mr_+}, \quad (2.22)$$

and r_+ to indicate the position of the horizon [note that $r_+(a = M) = M$]. Normalizing Eq. 2.21 by L , we find

$$a\Omega_R \leq (\mu/2)(a/M) \leq 1/2. \quad (2.23)$$

Even for the upper bound $a\Omega_R = 1/2$, the relative accuracy of Eq. (2.19) is still better than 0.2%.

2. Complex A_{lm} for a complex ω

To solve for the next-to-leading-order corrections to A_{lm} , we must compute the imaginary part A_{lm}^I . Because $\omega_I \ll \omega_R$,

when we allow $\omega = \omega_R - i\omega_I$ to be a complex number in the angular eigenvalue problem (2.4), we can treat the term linear in ω_I as a perturbation to the angular equation. Using the perturbation theory of eigenvalue equations, we find that

$$A_{lm}^I = -2a^2 \omega_R \omega_I \langle \cos^2 \theta \rangle, \quad (2.24)$$

where

$$\begin{aligned} \langle \cos^2 \theta \rangle &= \frac{\int \cos^2 \theta |u_\theta|^2 \sin \theta d\theta}{\int |u_\theta|^2 \sin \theta d\theta} \\ &= \frac{\int_{\theta_-}^{\theta_+} \frac{\cos^2 \theta}{\sqrt{a^2 \omega_R^2 \cos^2 \theta - \frac{m^2}{\sin^2 \theta} + A_{lm}^R}} d\theta}{\int_{\theta_-}^{\theta_+} \frac{1}{\sqrt{a^2 \omega_R^2 \cos^2 \theta - \frac{m^2}{\sin^2 \theta} + A_{lm}^R}} d\theta}. \end{aligned} \quad (2.25)$$

By taking the derivative of both sides of the Bohr-Sommerfeld condition (2.14) with respect to the variable $z = a\omega_R$ and by treating A_{lm} as a function of z , we can rewrite the above expression as

$$\langle \cos^2 \theta \rangle = -\frac{1}{2z} \left. \frac{\partial A_{lm}^R(z)}{\partial z} \right|_{z=a\omega_R}. \quad (2.26)$$

Substituting this expectation value into Eq. (2.24), we find

$$A_{lm}^I = a\omega_I \left[\frac{\partial A_{lm}^R(z)}{\partial z} \right]_{z=a\omega_R}. \quad (2.27)$$

Equation (2.27) defines a numerical prescription for computing $A_{lm} = A_{lm}^R + iA_{lm}^I$. This approach is quite natural: as ω becomes complex, A_{lm} is the analytic function whose value on the real axis is given by A_{lm}^R . The approximate formula (2.19), therefore, becomes

$$A_{lm} \approx L^2 - \frac{a^2 \omega^2}{2} \left[1 - \frac{m^2}{L^2} \right], \quad (2.28a)$$

or

$$\alpha \approx 1 - \frac{a^2 \Omega^2}{2} (1 - |\mu|^2), \quad (2.28b)$$

for a complex frequency ω .

C. The radial eigenvalue problem

Now that we have solved for the angular eigenvalues A_{lm} in terms of ω , we turn to the radial Teukolsky equation. From Eq. (2.5a), we see that the radial equation is already in the form

$$\frac{d^2 u_r}{dr_*^2} + V^r u_r = 0, \quad (2.29a)$$

if we define

$$V^r(r, \omega) = \frac{[\omega(r^2 + a^2) - ma]^2 - \Delta [A_{lm}(a\omega) + a^2 \omega^2 - 2ma\omega]}{(r^2 + a^2)^2}. \quad (2.29b)$$

Note here that V^r is an analytic function of ω , and that it is real-valued when ω is real.

In general, the WKB approximant for u_r is given at leading order by

$$u_r = b_+ e^{i \int^{r_*} \sqrt{V^r(r'_*)} dr'_*} + b_- e^{-i \int^{r_*} \sqrt{V^r(r'_*)} dr'_*}, \quad (2.30)$$

although in order to obtain a mode which is outgoing at $r_* \rightarrow +\infty$ (the same as $r \rightarrow \infty$) and ingoing at $r_* \rightarrow -\infty$ ($r \rightarrow r_+$), we must have

$$u_r = b_+ e^{i \int^{r_*} \sqrt{V^r(r'_*)} dr'_*}, \quad (2.31a)$$

for the region containing $r \rightarrow +\infty$, and

$$u_r = b_- e^{-i \int^{r_*} \sqrt{V^r(r'_*)} dr'_*}, \quad (2.31b)$$

for the region containing $r_* \rightarrow -\infty$. Intuitively speaking, a solution to Eq. (2.29a) will satisfy the asymptotic behavior above if $V^r \approx 0$ around a point $r = r_0$, and $V_r > 0$ on both sides. Then, the WKB expansion (2.30) is valid in the two regions on both sides of $r = r_0$, and the solution in the vicinity of r_0 must be obtained separately by matching to the WKB approximation. The matching will constrain the frequency, thereby giving a method to determine ω . A detailed calculation of this procedure has been carried out by Iyer and Will [11] to high orders in the WKB approximation; the only difference between our calculation and their result at lower orders comes from the more complex dependence of V^r on ω in our case (particularly because A_{lm} depends on ω in a more involved way).

1. Computing ω_R

From Iyer and Will [11], the conditions at the leading and next-to-leading order that must be solved to find ω_R are

$$V^r(r_0, \omega_R) = \left. \frac{\partial V^r}{\partial r} \right|_{(r_0, \omega_R)} = 0. \quad (2.32)$$

After a short calculation, these conditions can be expressed as

$$\Omega_R = \frac{\mu a}{r_0^2 + a^2} \pm \frac{\sqrt{\Delta(r_0)}}{r_0^2 + a^2} \beta(a\Omega_R), \quad (2.33a)$$

$$0 = \frac{\partial}{\partial r} \left[\frac{\Omega_R(r^2 + a^2) - \mu a}{\sqrt{\Delta(r)}} \right]_{r=r_0}, \quad (2.33b)$$

where we have defined

$$\beta(z) = \sqrt{\alpha(z) + z^2 - 2\mu z} \quad (2.34a)$$

$$\approx \sqrt{1 + \frac{z^2}{2} - 2\mu z + \frac{\mu^2 z^2}{2}}. \quad (2.34b)$$

In deriving Eq. (2.33b), we have used the fact that at $r > r_+$, $(r^2 + a^2)^2/\Delta$ is a monotonically increasing function, and, therefore the extrema of V^r are the same as those of $V^r(r^2 + a^2)^2/\Delta$; we then also used the fact that the quantity within the square brackets in Eq. (2.33b) is always nonzero at points at which $V^r = 0$.

One method of jointly solving Eqs. (2.33a) and (2.33b) would be to use Eq. (2.33b) to express Ω_R in terms of r_0

$$\Omega_R = \frac{(M - r_0)\mu a}{(r_0 - 3M)r_0^2 + (r_0 + M)a^2}, \quad (2.35)$$

and then insert this into Eq. (2.33a) to obtain r_0 ; finally Ω_R can be obtained by substituting this r_0 back into Eq. (2.35). If we use the approximate formula (2.34b) in this process, the equation for r_0 becomes a sixth-order polynomial in $x = r_0/M$, the roots of which can be found efficiently. For convenience, we write this polynomial here

$$2x^4(x-3)^2 + 4x^2[(1-\mu^2)x^2 - 2x - 3(1-\mu^2)](a/M)^2 + (1-\mu^2)[(2-\mu^2)x^2 + 2(2+\mu^2)x + (2-\mu^2)](a/M)^4. \quad (2.36)$$

For each pair $(\mu, a/M)$, there are in general two real roots for x , which correspond to the two possible values of r_0/M (and the two real frequencies with opposite signs).

Note that the procedure above will not work when $m = 0$ (when both the numerator and denominator of Eq. (2.35) vanish). In this case, we can directly require that

$$(r_p - 3M)r_p^2 + (r_p + M)a^2 = 0. \quad (2.37)$$

The solution, r_p can be inserted into Eq. (2.33a) and the result can be expressed in terms of elliptic integrals

$$\Omega_R(a, \mu = 0) = \pm \frac{\pi \sqrt{\Delta(r_p)}}{(r_p^2 + a^2) \text{EllipE} \left[\frac{a^2 \Delta(r_p)}{(r_p^2 + a^2)^2} \right]}, \quad (2.38)$$

where EllipE denotes an elliptic integral of the second kind. Here we have used the subscript p for this special case, because this mode will turn out to correspond to polar orbits.

We plot in Fig. 2 the relative error in Ω_R that comes from using the approximate expression for A_{lm} [Eq. (2.28a)] rather than the exact Bohr-Sommerfeld condition. The error is always less than $\sim 10^{-4}$ (we scale the quantity plotted on the vertical axis by 10^5), and therefore, we will use the approximate expression for A_{lm} for the remaining calculations involving Ω_R throughout this paper. In Fig. 3, we plot Ω_R for $a/M = 0, 0.3, 0.5, 0.9, 0.99$, and 1 (the flat curve corresponds to $a/M = 0$, and those with increasing slopes are the increasing values of a/M). While for low values of a/M below ~ 0.5 , Ω_R depends roughly linearly upon μ , for higher values of a/M (and for $\mu > 0$), Ω_R grows more rapidly than linearly. For $a/M = 1$, $\Omega_R \rightarrow 1/2$ when $\mu \rightarrow 1$, as anticipated.

2. Computing ω_I

At leading order, the imaginary part ω_I can be calculated using the same procedure set forth by Iyer and Will [11]. They

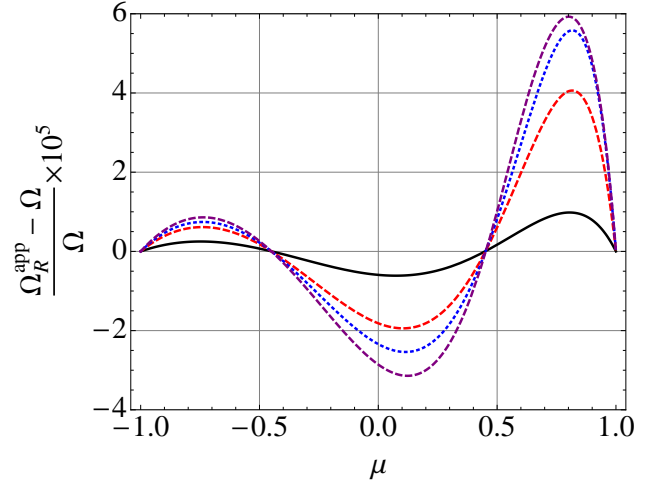


Figure 2: Difference in $\Omega_R(a, \mu)$ [Eq. (2.35)] that arises from using the approximate formula for A_{lm} [Eq. (2.28a)] as opposed to the exact formula. Here $a/M = 0.7, 0.9, 0.95$, and 0.99 correspond to black solid, red dashed, blue dotted, and purple long-dashed curves, respectively. The quantity plotted on the vertical axis has been scaled by 10^5 .

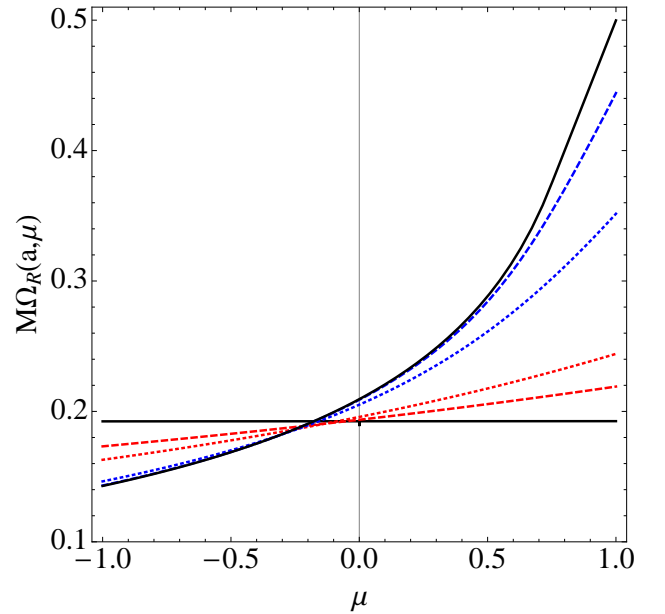


Figure 3: Real part of the QNM spectra from the WKB approximation. Black solid curves show Ω for $a/M = 0$ (the flat curve) and $a/M = 1$ (the curve that increases towards 0.5); red (light gray) dashed and dotted curves show $a/M = 0.3$ and 0.5 , while blue (dark gray) dotted and dashed curves show $a/M = 0.9$ and 0.99 .

find that

$$\begin{aligned} \omega_I &= -(n + 1/2) \frac{\sqrt{2 \left(\frac{d^2 V^r}{dr^2} \right)_{r_0, \omega_R}}}{\left(\frac{\partial V^r}{\partial \omega} \right)_{r_0, \omega_R}}, \\ &= -(n + 1/2) \Omega_I(a, \mu). \end{aligned} \quad (2.39)$$

In our calculation, we must also take into account that V^r also depends on ω through the angular eigenvalue's dependence

on ω . If we use the approximate formula for α , we obtain a reasonably compact expression for Ω_I :

$$\Omega_I = \Delta(r_0) \frac{\sqrt{4(6r_0^2\Omega_R^2 - 1) + 2a^2\Omega_R^2(3 - \mu^2)}}{2r_0^4\Omega_R - 4aMr_0\mu + a^2r_0\Omega_R[r_0(3 - \mu^2) + 2M(1 + \mu^2)] + a^4\Omega_R(1 - \mu^2)}. \quad (2.40)$$

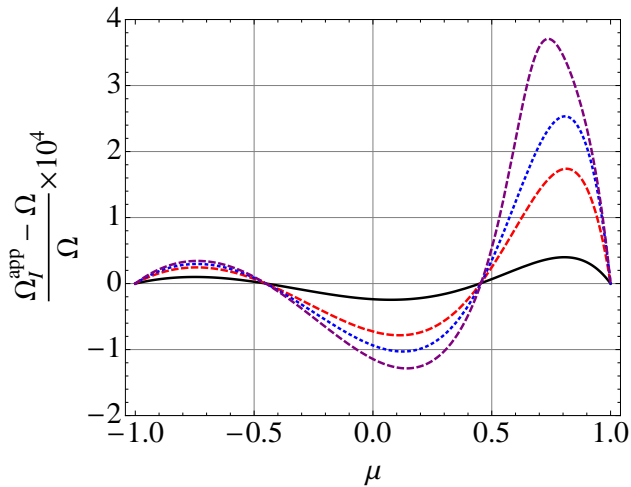


Figure 4: Difference in $\Omega_I(a, \mu)$ [Eq. (2.39)] from using the approximate formula for A_{lm} [Eq. (2.28a)] rather than the exact formula. Here $a/M = 0.7, 0.9, 0.95,$ and 0.99 correspond to black solid, red dashed, blue dotted, and purple long-dashed curves, respectively. We scale the quantity plotted along the vertical axis by 10^4 in this figure.

In Fig. 4, we plot the relative error in Ω_I from using the approximate formula for A_{lm} identically to that in Fig. 2 (although here we scale the quantity plotted on the vertical axis by 10^4). Because the error is always less than $\sim 10^{-3}$, we will use the approximate expression for A_{lm} for computing Ω_I in the remainder of this paper. In Fig. 5, we plot $\Omega_I(a, \mu)$ for several values of a/M (the same as those in Fig. 3, though not $a/M = 0.3$). The curve for $a/M = 0$ is flat, and those with larger spins have more rapidly decreasing slopes for increasing values of a/M . It is interesting to note that in the limit $a \rightarrow 1$, Ω_I becomes zero for values of μ in a finite interval $0.74 \lesssim \mu \leq 1$ (not only for $\mu = 1$ does Ω_I vanish). We will put forward an explanation for this phenomenon in Sec. IV, after we make connections between QNMs and wave propagation in the Kerr spacetime.

D. Accuracy of the WKB approximation

Because we calculated the leading and next-to-leading orders in the WKB approximation to ω_R , we expect that the relative error for increasing L should scale as $O(1/L^2)$. For the imaginary part, we computed only the leading-order expres-

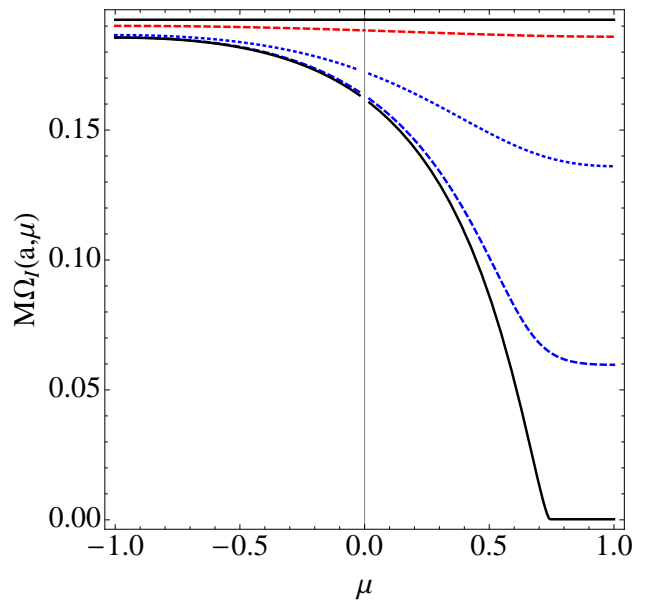


Figure 5: Imaginary part of the QNM spectrum computed in the WKB approximation. Black solid curves show Ω_I for $a/M = 0$ (again the flat curve) and $a/M = 1$ the curve that decreases and heads to zero. The red dashed curve shows $a/M = 0.5$, while blue dotted and dashed curves show $a/M = 0.9$ and 0.99 , respectively. For $a/M = 1$, modes with $\mu \gtrsim 0.74$ approach zero (modes that do not decay), while others still decay.

sion, and we would expect that the relative error might scale as $O(1/L)$. In addition, because at this order of approximation, we do not account for the spin of the wave, we anticipate that the error for the gravitational modes may be larger than those for scalar modes. In Figs. 6–9, we confirm most of these expectations, but we find the somewhat unexpected result that the relative error for the imaginary part also scales as $O(1/L^2)$.

In Fig. 6, we compare the WKB approximation to ω_R with numerical computations of the $s = 2$, gravitational-wave, quasinormal-mode spectra; specifically, we plot the fractional error against $\mu = m/L$, for $l = 2, 3, \dots, 14$, and for black holes of spins $a/M = 0.3, 0.5, 0.9,$ and 0.95 . The relative error clearly converges to $O(L^2)$. Even for $l = 2$, the relative error tends to be $\lesssim 30\%$, and at $l \geq 3$ the relative error stays below $\sim 1.5L^{-2}$ (this means error is $\lesssim 10\%$ for $l = 3$ and higher).

In Fig. 7, we compare the WKB spectra with $s = 0$ scalar quasinormal-mode spectra, for the same values of l and the same black-hole spins. We find a much better agreement. For

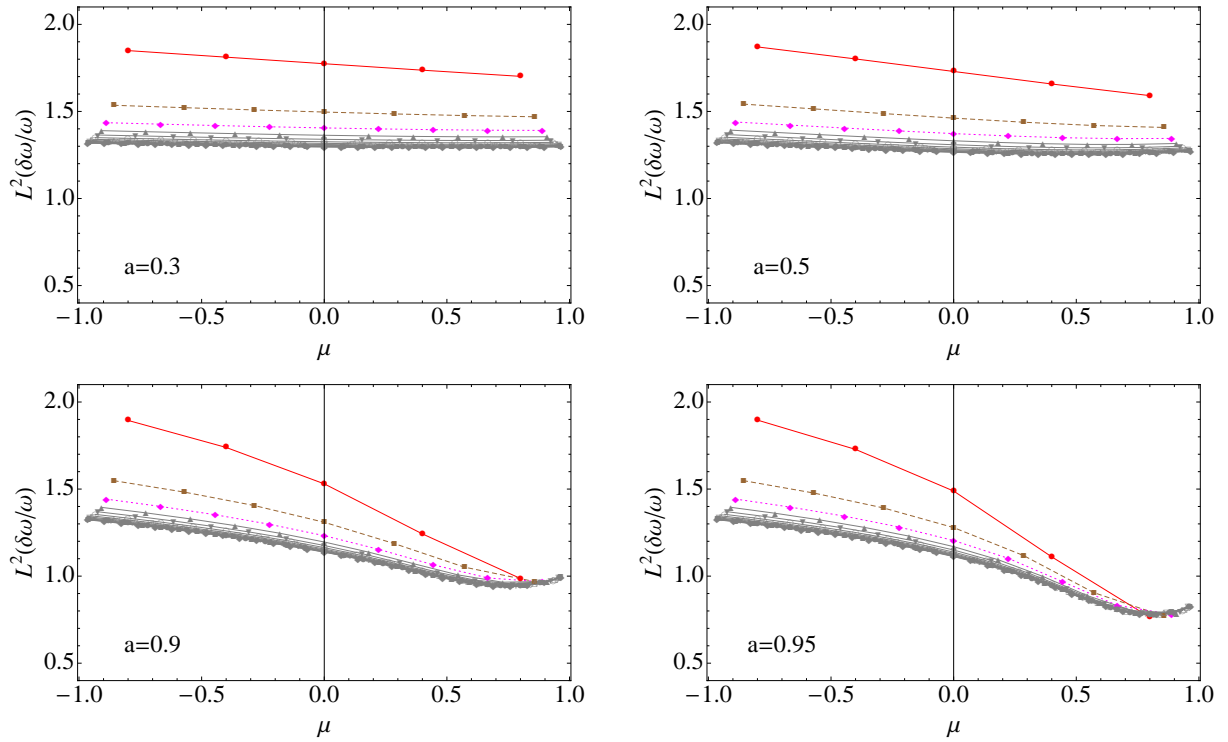


Figure 6: Fractional error, $\delta\omega_R/\omega_R$, of the WKB approximation to the $s = 2$, gravitational-wave, quasinormal-mode spectrum, multiplied by L^2 . The four panels correspond to four different spins which (going clockwise from the top left) are $a/M = 0.3, 0.5, 0.95$, and 0.9 . Errors for $l = 2, 3, 4$ are highlighted as red solid, brown dashed, and pink dotted lines, while the rest ($l = 5, \dots, 14$) are shown in gray. This shows that the relative error approaches the $O(1/L^2)$ scaling quite quickly.

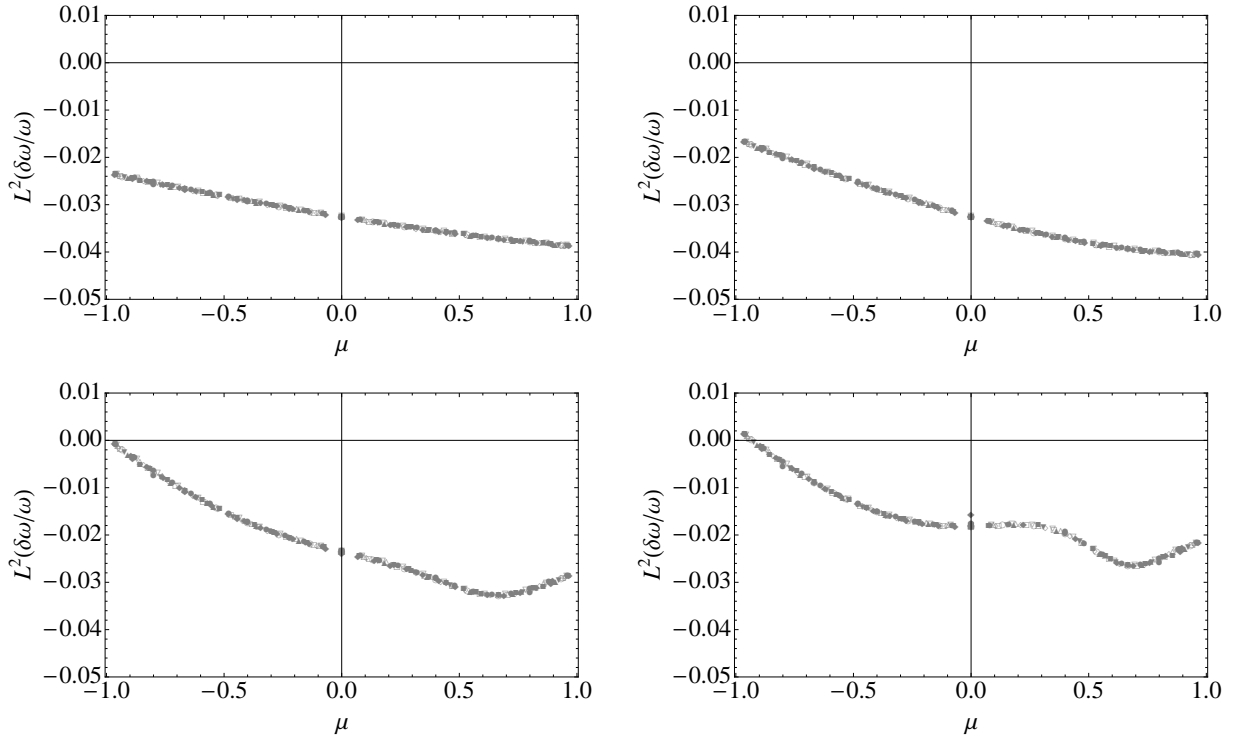


Figure 7: Fractional error, $\delta\omega_R/\omega_R$, of the WKB approximation to the $s = 0$, scalar-wave, quasinormal-mode spectrum, again scaled by L^2 . The four panels correspond to the same four spins in Fig. 6. The points shown in the four panels are for values of l in the range $l = 2, 3, \dots, 14$. Because all values of l nearly lie on the same curve, the relative error has converged at an order $O(1/L^2)$ even for very low l . The overall error is also significantly lower than that for the $s = 2$ modes.

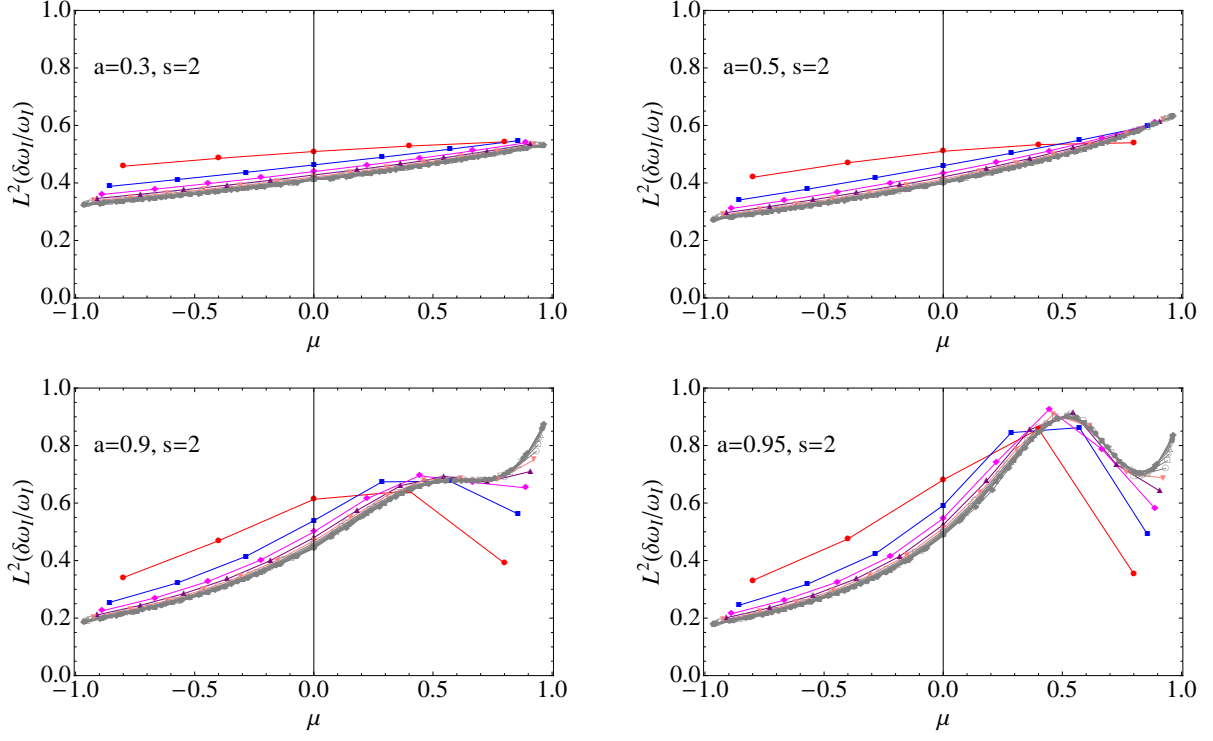


Figure 8: Fractional error, $\delta\omega_l/\omega_l$, of the WKB approximation to the $s = 2$, gravitational-wave, quasinormal-mode spectrum, also scaled by L^2 . The panels and the curves are plotted in the same way as in Fig. 6, and the error scales similarly.

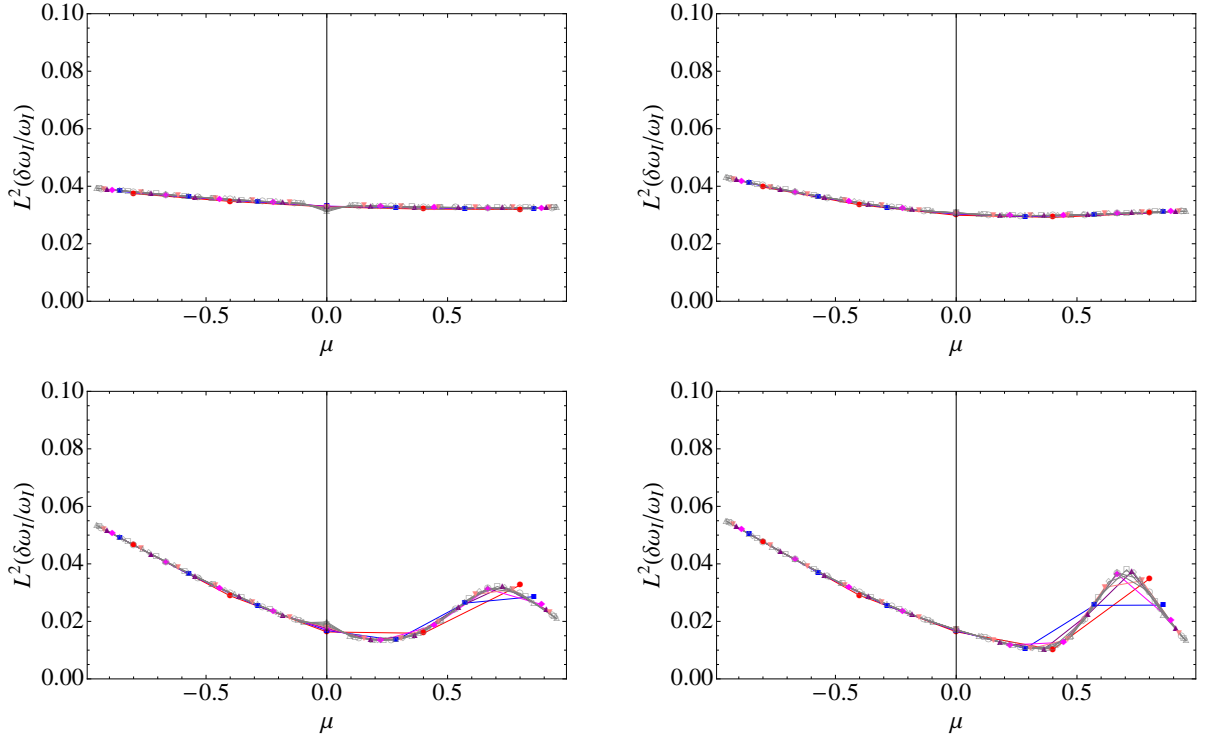


Figure 9: Fractional error, $\delta\omega_l/\omega_l$, of the WKB approximation to the $s = 0$, scalar-wave, quasinormal-mode spectrum, again multiplied by L^2 . The four panels and the points are shown in the same way as in Fig. 7, and there is a similar rapid convergence of the error.

all $l \geq 2$ modes, the relative error stays below $4 \times 10^{-2} L^{-2}$. This suggests that coupling between the spin of the wave (i.e., its tensor polarization) and the background curvature of the Kerr black hole is the main source of error in our WKB approximation.

In Figs. 8 and 9, we perform the same comparisons as in Figs. 6 and 7 for the imaginary part of frequency. Surprisingly, we find that for both $s = 0$ and 2, the relative error in ω_I is $O(L^{-2})$. For $s = 0$, the relative error is $\lesssim 6 \times 10^{-2} L^{-2}$, while for $s = 2$, the error is $\lesssim L^{-2}$.

With this comparison, we conclude our direct calculation of the QNM spectrum by WKB techniques. We will discuss additional features of the QNM spectrum in Sec. IV, but before doing so, we will develop a geometric interpretation of our WKB results. Doing so will help us to develop more intuition about our WKB expressions.

III. GEOMETRIC OPTICS IN THE KERR SPACETIME

In this section, we first briefly review the formalism of geometric optics, which describes the propagation of waves with reduced wavelengths λ that are much shorter than the space-time radius of curvature, R , and the size of the phase front, \mathcal{L} . In the geometric-optics approximation, the phase of the waves remains constant along null geodesics (rays), while the amplitude can be expressed in terms of the expansion and contraction of the cross-sectional area of bundles of null rays. We will then specialize the geometric-optics formalism to the Kerr spacetime, and we will write down the most general form of propagating waves in the geometric-optics approximation. Using the Hamilton-Jacobi method, we see that the waves' motion can be related to the null geodesics in the spacetime. By applying boundary conditions to the approximate wave, we obtain expressions for the quasinormal-mode waveforms and their corresponding complex frequency spectra and angular separation constants, in the eikonal limit.

A. Geometric optics: general theory

Here we briefly review the geometric-optics approximation to scalar-wave propagation (see, e.g., Section 22.5 of Ref. [35] for details). A massless scalar wave u propagating in curved spacetime satisfies the wave equation

$$g^{\mu\nu} \nabla_\mu \nabla_\nu u = 0. \quad (3.1)$$

If we write

$$u = A e^{i\Phi}, \quad (3.2)$$

then at leading order in λ/\mathcal{L} , we have

$$g^{\mu\nu} k_\mu k_\nu = 0, \quad k_\mu \equiv \partial_\mu \Phi, \quad (3.3)$$

while at next-to-leading order,

$$2k^\mu \partial_\mu \log A + \nabla_\mu k^\mu = 0. \quad (3.4)$$

Note that Eq. (3.3) also implies that k^μ is geodesic,

$$k^\mu \nabla_\mu k_\nu = k^\mu \nabla_\mu \nabla_\nu \Phi = k^\mu \nabla_\nu \nabla_\mu \Phi = k^\mu \nabla_\nu k_\mu = 0. \quad (3.5)$$

Equations (3.2)–(3.5) encode information about the transport of the amplitude A and phase Φ along a null geodesic (or a ray). The phase should be kept constant, because Eq. (3.3) states

$$k^\mu \partial_\mu \Phi = 0, \quad (3.6)$$

while the amplitude is transported along the ray in a manner that depends upon the propagation of neighboring rays. Because the 2D area, \mathcal{A} , of a small bundle of null rays around the central ray satisfies the equation

$$\nabla_\mu k^\mu = k^\mu \partial_\mu \log \mathcal{A}, \quad (3.7)$$

it is possible to show from Eq. (3.4) that

$$k^\mu \partial_\mu \left(\mathcal{A}^{1/2} A \right) = 0, \quad (3.8)$$

which implies $A \propto \mathcal{A}^{-1/2}$.

The transport equations (3.6) and (3.8) provide a way to construct a wave solution from a single ray; therefore, any solution to the wave equation (3.1) in a 4D spacetime region can be found from a three-parameter family of null rays (with smoothly varying initial positions and wave vectors) by assigning smoothly varying initial values of (Φ, A) and then transporting these values along the rays. (We use the phrase ‘‘smoothly varying’’ to mean that the values of (Φ, A) must change on the scale of $\mathcal{L} \gg \lambda$.) We note it is often convenient to divide the three-parameter family of initial positions of the null rays into two-parameter families of rays with constant initial values of Φ . The constant- Φ surfaces are the initial phase fronts, which, upon propagation along the rays, become 3D phase fronts of the globally defined wave. The more usual 2D phase fronts, at a given time, are obtained if we take a particular time slicing of the spacetime and find the 2D cross sections of the 3D phase fronts in this slicing.

The above formalism describes wave propagation up to next-to-leading order in \mathcal{L}/λ , which will be enough for us to build a geometric correspondence for both the real frequency, the decay rate, and the angular separation constant of QNMs in the Kerr spacetime.

B. Null geodesics in the Kerr spacetime

Now let us review the description of null geodesics in the Kerr spacetime using the Hamilton-Jacobi formalism. In general, the Hamilton-Jacobi equation states

$$g^{\mu\nu} (\partial_\mu S)(\partial_\nu S) = 0, \quad (3.9)$$

where $S(x^\mu)$ is called the *principal function*. For the Kerr spacetime, the Hamilton-Jacobi equation can be solved via separation of variables (see, e.g., [34]), through which the principal function can be expressed as

$$S(t, \theta, \phi, r) = S_\theta(\theta) + L_z \phi + S_r(r) - \mathcal{E}t, \quad (3.10)$$

where \mathcal{E} and L_z are constants that are conserved because of the the timelike and axial Killing vectors of the Kerr spacetime. Physically, \mathcal{E} and L_z represent the energy and z -directed specific angular momentum of the massless scalar particle. The functions $S_r(r)$ and $S_\theta(\theta)$ are given by

$$S_r(r) = \int^r \frac{\sqrt{\mathcal{R}(r')}}{\Delta(r')} dr', \quad S_\theta(\theta) = \int^\theta \sqrt{\Theta(\theta')} d\theta', \quad (3.11a)$$

where $\mathcal{R}(r)$ and $\Theta(\theta)$ are given by

$$\mathcal{R}(r) = [\mathcal{E}(r^2 + a^2) - L_z a]^2 - \Delta[(L_z - a\mathcal{E})^2 + \mathcal{Q}], \quad (3.11b)$$

$$\Theta(\theta) = \mathcal{Q} - \cos^2 \theta (L_z^2 / \sin^2 \theta - a^2 \mathcal{E}^2), \quad (3.11c)$$

and $\Delta(r)$ is given in Eq. (2.5d). The constant \mathcal{Q} is the Carter constant of the trajectory, which is a third conserved quantity along geodesics in the Kerr spacetime.

The principal function $S(x^\mu; \mathcal{E}, L_z, \mathcal{Q})$ contains information about all null geodesics; equations of motion for individual null geodesics are given by first choosing a particular set of $(\mathcal{E}, L_z, \mathcal{Q})$, and then imposing

$$\frac{\partial S}{\partial \mathcal{E}} = 0, \quad \frac{\partial S}{\partial L_z} = 0, \quad \frac{\partial S}{\partial \mathcal{Q}} = 0. \quad (3.12)$$

These conditions lead to a set of first-order differential equations

$$\frac{dt}{d\lambda} = \frac{r^2 + a^2}{\Delta} [\mathcal{E}(r^2 + a^2) - L_z a] - a(a\mathcal{E} \sin^2 \theta - L_z), \quad (3.13a)$$

$$\frac{d\phi}{d\lambda} = - \left(a\mathcal{E} - \frac{L_z}{\sin^2 \theta} \right) + \frac{a [\mathcal{E}(r^2 + a^2) - L_z a]}{\Delta}, \quad (3.13b)$$

$$\frac{dr}{d\lambda} = \sqrt{\mathcal{R}}, \quad \frac{d\theta}{d\lambda} = \sqrt{\Theta}, \quad (3.13c)$$

where we have defined

$$\frac{d}{d\lambda} \equiv \Sigma \frac{d}{d\zeta}, \quad \Sigma = r^2 + a^2 \cos^2 \theta, \quad (3.14)$$

and ζ is an affine parameter along the null geodesics.

C. Correspondence with quasinormal modes

Here we will find connection between the general set of wave solutions in the previous section, and the particular solutions that correspond to a quasinormal modes, in the geometric-optics limit. Specifically, we will look for waves that propagate outwards at infinity and down the horizon. With this correspondence, we will be able to make a geometric interpretation of our WKB results from Sec. II.

1. Leading order: conserved quantities of rays and the real parts of quasinormal-mode parameters

It is straightforward to note that the Hamilton-Jacobi equation (3.9) is identical to the leading-order geometric-optics

equations, if we identify the phase, Φ , with the principal function, S . Therefore, at leading order, we can write

$$u = e^{iS} = e^{-i\mathcal{E}t} e^{iL_z \phi} e^{\pm iS_\theta} e^{\pm iS_r}, \quad (3.15)$$

where we recall that the amplitude A differs from unity only at next-to-leading order (we will treat it in the next subsections). Here, we have a chosen set of conserved quantities, $(\mathcal{E}, \mathcal{Q}, L_z)$, to identify the wave we wish to connect with a quasinormal-mode solution. The region in which the wave propagates is identical to the region in which geodesics with these conserved quantities can propagate. In addition, for each point in this region, there is one (and only one) geodesic passing through it; that we have \pm in front of S_θ and S_r means only that either propagation direction could be a solution to the wave equation.

Now we note that u , a scalar wave in the Kerr spacetime, must separate as in Eq. (2.3). By comparing Eq. (2.3) and Eq. (3.15), we can immediately identify that

$$\mathcal{E} = \omega_R. \quad (3.16)$$

Because \mathcal{E} is a real quantity (the conserved energy of the null geodesic), we see that at leading order, the wave does not decay. Next, we also observe that in order for u to be consistently defined in the azimuthal direction, L_z (of the null geodesics that S describes) must be an integer. This allows us to make the second identification

$$L_z = m. \quad (3.17)$$

Comparing S_θ from Eq. (3.11a) and u_θ from Eqs. (2.12) and (2.7b) (focusing on one direction of θ propagation, and ignoring next-to-leading-order terms), we can also conclude that

$$\mathcal{Q} = A_{lm}^R - m^2. \quad (3.18)$$

At this stage, given any set of $(\mathcal{E}, \mathcal{Q}, L_z)$, we will be able to find a wave solution that exists in the region in which the geodesics travel. Not all such sets of conserved quantities correspond to quasinormal modes, however, because they may not satisfy the correct boundary conditions of QNMs.

We will first explain the conditions on the radial motion of the geodesics that will allow these particular geodesics to correspond to a wave that satisfies outgoing and downgoing conditions at $r_* \rightarrow \pm\infty$, respectively. If the radial geodesics satisfy $\mathcal{R} > 0$ everywhere, then there will be traveling waves across the entire r_* axis, which will not satisfy the boundary conditions; if there are two disconnected regions of traveling waves, however, waves will scatter off the potential on each side, and they will also fail to satisfy the boundary conditions. The only way to satisfy the boundary conditions is to have a point r_0 at which $\mathcal{R} = 0$ and $\mathcal{R}' = 0$, in which case there will be a family of geodesics on each side of $r = r_0$ (with each member a *homoclinic orbit* which has $r \rightarrow r_0$ on one end) and a *spherical orbit* with constant $r = r_0$. The corresponding wave has zero radial spatial frequency at $r = r_0$, and this frequency increases towards $r < r_0$ and decreases towards $r > r_0$. Noting that

$$\mathcal{R} = V^r (r^2 + a^2)^2, \quad (3.19)$$

Table I: Geometric-optics correspondence between the parameters of a quasinormal mode, $(\omega, A_{lm}, l, \text{ and } m)$, and the conserved quantities along geodesics, $(\mathcal{E}, L_z, \text{ and } \mathcal{Q})$. To establish a correspondence with the next-to-leading-order, geometric-optics approximation, the geodesic quantities \mathcal{E} and \mathcal{Q} must be complex.

Wave Quantity	Ray Quantity	Interpretation
ω_R	\mathcal{E}	Wave frequency is same as energy of null ray (determined by spherical photon orbit).
m	L_z	Azimuthal quantum number corresponds to z angular momentum (quantized to get standing wave in ϕ direction).
A_{lm}^R	$\mathcal{Q} + L_z^2$	Real part of angular eigenvalue related to Carter constant (quantized to get standing wave in θ direction).
ω_I	$\gamma = -\mathcal{E}_I$	Wave decay rate is proportional to Lyapunov exponent of rays neighboring the light sphere.
A_{lm}^I	\mathcal{Q}_I	Nonzero because $\omega_I \neq 0$ (see Secs. II B 2 and III C 3 for further discussion).

the condition

$$\mathcal{R} = \mathcal{R}' = 0 \quad (3.20)$$

is the same as the condition, Eq. (2.32), which determines ω_R in terms of L and m in the WKB approximation. It is worth mentioning that although the condition of Eq. (3.20) imposed on $(\mathcal{E}, \mathcal{Q}, L_z)$ can be interpreted most easily as the condition for a spherical photon orbit, the wave function for the quasinormal mode we are considering is *not* localized around that orbit. The wave function at leading order, in fact, has a constant magnitude at every location that homoclinic orbits reach (i.e., the entire r axis). We will derive the amplitude corrections in the next section.

The quantization of the frequency ω_R in terms of the multipolar indices l and m arises from the quantization of the motion in the angular directions. For the azimuthal direction, it is easy to see that for the wave function to be single-valued, we need to impose $L_z = m \in \mathbb{Z}$. For the θ direction, we note that

$$\Theta = V^\theta \sin^2 \theta, \quad (3.21)$$

and the θ -quantization condition for the wave, Eq. (2.14), is

$$\int_{\theta_-}^{\theta_+} \sqrt{\Theta} d\theta = (L - |m|)\pi. \quad (3.22)$$

This corresponds to the Bohr-Sommerfeld condition for a particle moving in a potential given by Θ . Consequently, the condition for a standing wave along the θ direction (at leading order) is equivalent to

$$\begin{aligned} \mathcal{Q} &= A_{lm}(\omega_R a) - m^2 \\ &\approx L^2 - m^2 - \frac{a^2 \omega_R^2}{2} \left[1 - \frac{m^2}{L^2} \right]. \end{aligned} \quad (3.23)$$

In summary, we connected the QNM's wave function to the Hamilton-Jacobi principal function of homoclinic null geodesics (at leading order). These geodesics have the same energy, Carter constant, and z -component of its angular momentum as a spherical photon orbit; however only spherical

orbits with *quantized* Carter constants and z -angular momenta correspond to quasinormal modes. In Table I, we summarize our geometric-optics correspondence; so far we have identified the first three entries on the table. We can find the next two correspondences by investigating next-to-leading-order geometric optics in the next part.

2. Next-to-leading order: radial amplitude corrections and the imaginary part of the frequency

We showed in the previous part that the conserved quantities of a spherical photon orbit, $(\mathcal{E}, \mathcal{Q}, L_z)$, correspond simply to the real parts of the quasinormal-mode parameters, (ω_R, A_{lm}^R, m) , which are the leading-order quantities of a quasinormal mode. Here, we will show that the behavior of the homoclinic orbits—namely, how the orbits propagate away from the spherical orbit, and how they move between θ_\pm —reveals the spatiotemporal variation of the wave (i.e. the decay rate and the shape of its wave function in space). In Fig. 10, we plot the trajectory of a particular series of homoclinic orbits on the r - θ plane, to which we will refer at several points in the discussion below.

With the appropriate values of $(\mathcal{E}, \mathcal{Q}, L_z)$, the function u in Eq. (3.15) solves the wave equation to leading order and satisfies the required boundary conditions. To recover the decaying behavior of quasinormal modes, however, we make corrections to the amplitude of the wave, which appear at next-to-leading order in the geometric-optics approximation. Because of symmetry, there should not be any correction to the amplitude in the ϕ direction, and the correction in the t direction should be a simple decay; therefore, we write

$$u = A \exp(iS) = \underbrace{e^{-\gamma t} A_r(r) A_\theta(\theta)}_{A(t,r,\theta)} e^{-i\mathcal{E}t} e^{iL_z \phi} e^{\pm iS_\theta} e^{\pm iS_r}. \quad (3.24)$$

This general expression contains four possible directions that the wave could be propagating: the $\pm\theta$ direction and the $\pm r$ direction (depending on the signs in front of S_r and S_θ). Because the boundary conditions require that the waves propa-

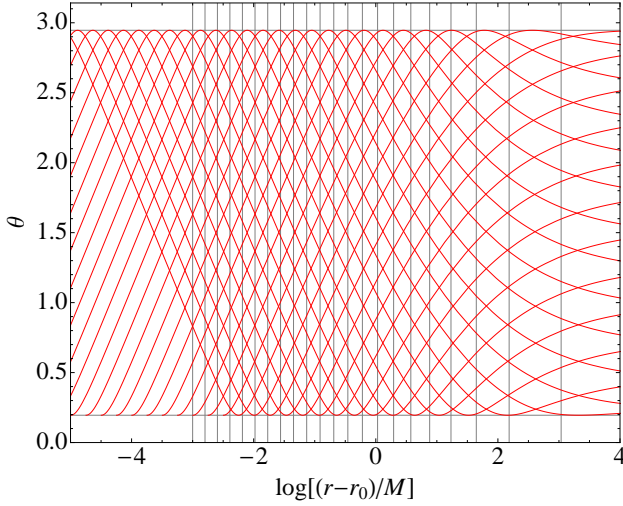


Figure 10: Schematic plot of trajectories in the r - θ plane of homoclinic orbits outside of the peak of the potential (specifically for a black hole with spin $a/M = 0.7$ and a photon orbit with radius $r_0/M = 2.584$). The two horizontal grid lines mark the turning points, $\theta = \theta_{\pm}$; between these turning points, there are two homoclinic orbits passing through every point, while at turning points only one orbit passes through. Vertical grid lines indicate when the value of parameter λ has changed along the orbit by (an arbitrarily chosen value) $\Delta\lambda = 0.046M$. Near the spherical photon orbit, each homoclinic orbit undergoes an infinite number of periodic oscillations in θ while $r - r_0$ is growing exponentially as a function of λ .

gate towards $r_* \rightarrow +\infty$ for $r > r_0$ and $r_* \rightarrow -\infty$ for $r < r_0$, the sign in front of S_r should be positive for $r > r_0$ and negative for $r < r_0$. For θ motion, however, we insist that both directions (signs) be present, because a quasinormal mode is a standing wave in the θ direction. Focusing on $r > r_0$, we write

$$u = e^{-\gamma} A_r(r) [A_{\theta}^+ e^{iS_{\theta}} + A_{\theta}^- e^{-iS_{\theta}}] e^{-i\mathcal{E}t + iL_z \phi + iS_r} \equiv u_+ + u_- . \quad (3.25)$$

We will next require that both u_+ and u_- satisfy the wave equation to next-to-leading order, separately. By explicitly computing Eq. (3.4) (or $A\sqrt{\mathcal{A}} = \text{const}$) in the Kerr spacetime, we find the amplitude satisfies the relation

$$\Sigma \frac{d \log A}{d \zeta} = -\frac{1}{2} \left[\partial_r (\Delta(r) \partial_r S_r) + \frac{1}{\sin \theta} \partial_{\theta} (\sin \theta \partial_{\theta} S_{\theta}) \right]. \quad (3.26)$$

Here ζ is an affine parameter along the geodesic specified by $(\mathcal{E}, \mathcal{Q}, L_z)$. If we use the parameter λ defined by $d/d\lambda = \Sigma d/d\zeta$ then we can separate the left-hand side of the equation as

$$\Sigma \frac{d \log A}{d \zeta} = \frac{d}{d\lambda} \log A_r(r) + \frac{d}{d\lambda} \log A_{\theta}(\theta) - \gamma \frac{dt}{d\lambda}. \quad (3.27)$$

Because the right-hand side of Eq. (3.13a) for $dt/d\lambda$, separates into a piece that depends only upon r and one that depends only upon θ , we will write Eq. (3.13a) schematically

as

$$\frac{dt}{d\lambda} = \bar{i} + \tilde{i}, \quad (3.28)$$

where \bar{i} is only a function of r and \tilde{i} is only a function of θ . Unlike in Eq. (3.13a), we will require that \tilde{i} average to zero when integrating over λ for half a period of motion in the θ direction (i.e., from θ_- to θ_+). We can ensure this condition is satisfied by subtracting an appropriate constant from \tilde{i} and adding it to \bar{i} . Combining Eqs. (3.26)–(3.28) and performing a separation of variables, we obtain

$$\sqrt{\mathcal{R}} \frac{d \log A_r}{dr} - \bar{\gamma} \bar{i} = -\frac{\mathcal{R}'}{4\sqrt{\mathcal{R}}}, \quad (3.29a)$$

$$\sqrt{\Theta} \frac{d \log A_{\theta}^{\pm}}{d\theta} \mp \tilde{\gamma} \tilde{i} = -\frac{1}{2 \sin \theta} (\sqrt{\Theta} \sin \theta)', \quad (3.29b)$$

where a prime denotes a derivative with respect to r for functions of r only, and a derivative with respect to θ for functions of θ only (whether it is a θ or r derivative should be clear from the context). While it might at first seem possible to add a constant to the definition of \tilde{i} , and subtract it from \bar{i} and still have both u_+ and u_- satisfy the next-to-leading order geometric optics, because we have already chosen to have \tilde{i} average to zero,

$$\int_{\theta_-}^{\theta_+} \tilde{\gamma} \frac{d\theta}{\sqrt{\Theta}} = \int \tilde{\gamma} d\lambda = 0, \quad (3.30)$$

this separation is the only way to guarantee that $|A_{\theta}^{\pm}|$ match each other at both ends. We will discuss the angular wave function in greater detail in the next part of this section.

Let us now turn to the radial equation, from which we will be able to compute the decay rate. Close to r_0 , we can expand $\mathcal{R}(r)$ to leading order as

$$\mathcal{R}(r) \approx \frac{(r-r_0)^2}{2} \mathcal{R}''(r_0). \quad (3.31)$$

Substituting this result into Eq. (3.29a), we find

$$\frac{d \log A_r}{dr} = \frac{1}{r-r_0} \left[\bar{\gamma} \sqrt{\frac{2}{\mathcal{R}''(r_0)}} - \frac{1}{2} \right], \quad (3.32)$$

where we used the notation $\mathcal{R}_0'' \equiv \mathcal{R}''(r_0)$. For A_r to be a function that scales as $A_r \sim (r-r_0)^n$ around r_0 for some integer n (namely it scales like a well-behaved function), we need to have

$$\begin{aligned} \gamma &= \left(n + \frac{1}{2} \right) \frac{\sqrt{\mathcal{R}_0''/2}}{\bar{i}} \\ &= (n+1/2) \lim_{r \rightarrow r_0} \frac{1}{r-r_0} \frac{dr/d\lambda}{\langle dt/d\lambda \rangle_{\theta}}. \end{aligned} \quad (3.33)$$

To arrive at the second line, we used Eq. (3.31), the fact that $dr/d\lambda = \sqrt{\mathcal{R}}$, and that \bar{i} is the part of $dt/d\lambda$ that does not vanish when averaging over one cycle of motion in the θ direction; the limit in the expression comes from the fact that the approximation in Eq. (3.31) becomes more accurate as $r \rightarrow r_0$.

The physical interpretation of the rate that multiplies $(n + 1/2)$ is somewhat subtle. Because the θ motion is independent from r motion, a bundle of geodesics at the same r slightly larger than r_0 , but at different locations in θ , will return to their respective initial values of θ with a slightly increased value of r after one period of motion in the θ direction. The area of this bundle increases in the process, and by Eq. 3.8, the amplitude of the wave must decay; the rate of decay is governed by the quantity that multiplies $(n + 1/2)$ in Eq. (3.33).

In addition, as shown in Fig. 10, the homoclinic orbits do pass through an infinite number of such oscillations near r_0 , because the radial motion is indefinitely slower than the θ motion as r approaches r_0 . It is clear from Fig. 10 that

$$\frac{1}{r-r_0} \frac{\Delta r}{\Delta \lambda} = \frac{\Delta \log(r-r_0)}{\Delta \lambda} \quad (3.34)$$

approaches a constant as $r \rightarrow r_0$. By multiplying the above equation by the constant value of $(\Delta \lambda)/(\Delta t)$ over one orbit of motion in the θ direction,

$$\frac{1}{r-r_0} \frac{\Delta r}{\Delta t} = \frac{\Delta \log(r-r_0)}{\Delta t} \equiv \gamma_L \quad (3.35)$$

also approaches a constant. This is usually defined as the *Lyapunov exponent* of one-dimensional motion; here, however, we emphasize that it is defined only after averaging over entire cycle of θ motion. By comparing Eq. (3.35) with the second line of Eq. (3.33), and bearing in mind that the Lyapunov exponent is defined after averaging over one period of θ motion, one can write Eq. (3.33) as

$$\gamma = (n + \frac{1}{2})\gamma_L. \quad (3.36)$$

To put Eq. (3.33) into a form that relates more clearly to Eq. (2.39), we use the conditions on the phase function,

$$\frac{\partial S}{\partial \mathcal{E}} = 0, \quad \frac{\partial S}{\partial \mathcal{Q}} = 0, \quad (3.37)$$

which hold for any point on the trajectory of the particle. We will apply this condition to two points on the particle's trajectory: one at (t, r, θ, ϕ) and the second at $(t + \Delta t, r + \Delta r, \theta, \phi + \Delta \phi)$, where Δt is chosen such that the particle completes a cycle in θ in this time (and it moves to a new location shifted Δr and $\Delta \phi$). Substituting in the explicit expressions for the principal function in Eqs. (3.10) and (3.11a), we find

$$\frac{\partial}{\partial \mathcal{E}} \left[\int_r^{r+\Delta r} \frac{\sqrt{\mathcal{R}(r')}}{\Delta(r')} dr' + \Delta S_\theta \right] = \Delta t \quad (3.38a)$$

$$\frac{\partial}{\partial \mathcal{Q}} \left[\int_r^{r+\Delta r} \frac{\sqrt{\mathcal{R}(r')}}{\Delta(r')} dr' + \Delta S_\theta \right] = 0. \quad (3.38b)$$

where we have defined

$$\Delta S_\theta \equiv 2 \int_{\theta_-}^{\theta_+} \sqrt{\Theta(\theta')} d\theta' \equiv \oint \sqrt{\Theta(\theta')} d\theta'. \quad (3.39)$$

Because the change Δr is infinitesimal for r near r_0 , the integrand is roughly constant, and the r -dependent part of the

integral becomes the product of the integrand with Δr . Then, one can use Eq. (3.31) to write Eqs. (3.38a) and (3.38b) as

$$\frac{1}{\sqrt{2\mathcal{R}_0''}\Delta_0} \frac{\partial \mathcal{R}}{\partial \mathcal{E}} \frac{\Delta r}{r-r_0} + \frac{\partial \Delta S_\theta}{\partial \mathcal{E}} = \Delta t, \quad (3.40a)$$

$$\frac{1}{\sqrt{2\mathcal{R}_0''}\Delta_0} \frac{\partial \mathcal{R}}{\partial \mathcal{Q}} \frac{\Delta r}{r-r_0} + \frac{\partial \Delta S_\theta}{\partial \mathcal{Q}} = 0. \quad (3.40b)$$

Now, we also note that for a given fixed $L_z = m$, the angular Bohr-Sommerfeld condition in Eq. (3.22) makes \mathcal{Q} a function of \mathcal{E} through the condition that $\Delta S_\theta = (L - |m|)\pi$. Because ΔS_θ is a function of \mathcal{E} , its total derivative with respect to \mathcal{E} must vanish,

$$\frac{\partial \Delta S_\theta}{\partial \mathcal{E}} + \frac{\partial \Delta S_\theta}{\partial \mathcal{Q}} \left(\frac{d\mathcal{Q}}{d\mathcal{E}} \right)_{\text{BS}} = 0. \quad (3.41)$$

Therefore, when we multiply Eq. (3.40b) by $(d\mathcal{Q}/d\mathcal{E})_{\text{BS}}$ and add it to Eq. (3.40a), we obtain the condition that

$$\frac{1}{\sqrt{2\mathcal{R}_0''}\Delta_0} \left[\frac{\partial \mathcal{R}}{\partial \mathcal{E}} + \frac{\partial \mathcal{R}}{\partial \mathcal{Q}} \left(\frac{d\mathcal{Q}}{d\mathcal{E}} \right)_{\text{BS}} \right] \frac{\Delta r}{r-r_0} = \Delta t. \quad (3.42)$$

Combining this fact with the definition of the Lyapunov exponent in Eq. (3.35) and Eq. (3.36), we find that

$$\gamma = \left(n + \frac{1}{2} \right) \frac{\sqrt{2\mathcal{R}_0''}\Delta_0}{\left[\frac{\partial \mathcal{R}}{\partial \mathcal{E}} + \frac{\partial \mathcal{R}}{\partial \mathcal{Q}} \left(\frac{d\mathcal{Q}}{d\mathcal{E}} \right)_{\text{BS}} \right]_{r_0}}, \quad (3.43)$$

where we recall that the quantities should be evaluated at r_0 . Equation (3.43) is equivalent to Eq. (2.39). Note, however, that in Eq. (3.43) we explicitly highlight the dependence of \mathcal{Q} on \mathcal{E} through the term $(d\mathcal{Q}/d\mathcal{E})_{\text{BS}}$. There is an analogous term in Eq. (2.39) from the dependence of A_{lm} on ω in the expression for the potential V^r , which we must take into account when computing $\partial V^r / \partial \omega$; however, we did not write it out explicitly in Eq. (2.39).

Summarizing the physical interpretation of the results in this subsection, we note that the Lyapunov exponent γ_L is the rate at which the cross-sectional area of a bundle of homoclinic rays expand, when averaged over one period of motion in the θ direction in the vicinity of r_0 . The spatial Killing symmetry along ϕ means the extension of the ray bundle remains the same along that direction. This, therefore, allows us to write

$$\mathcal{A} \sim e^{\gamma_L t}. \quad (3.44)$$

Correspondingly, the $A\sqrt{\mathcal{A}} = \text{const}$ law requires that

$$A \sim e^{-\gamma_L t/2}, \quad (3.45)$$

which agrees with the decay rate of the least-damped QNM. The higher decay rates given by Eq. (3.33) come from an effect related to the intrinsic expansion of the area of a phase front. More specifically, if the amplitude is already nonuniform at points with different $r - r_0$ (but same θ), then shifting the spatial locations of the nonuniform distribution gives the appearance of additional decay.

3. *Next-to-leading order: angular amplitude corrections and the imaginary part of Carter's constant*

Having found a relation in Eq. (3.29a) between the imaginary part of the energy, ω_I , and the rate of divergence of rays, we now turn to Eq. (3.29b) to understand the geometric meaning of the complex part of A_{lm} . We recall from Sec. III C 1 that $\mathcal{Q} = A_{lm}^R - m^2$, at leading order, for a real Carter constant \mathcal{Q} . Because A_{lm} becomes complex at next to leading order (and because m remains unchanged), if the correspondence $\mathcal{Q} = A_{lm} - m^2$ holds for a complex A_{lm} , then the Carter constant should also be complex, and its imaginary part should be equivalent to A_{lm}^I . In this part, we argue that this relationship holds.

By integrating Eq. (3.29b), we find that

$$A_{\theta}^{\pm} = \sqrt{\frac{1}{\sin \theta \sqrt{\Theta}}} \exp \left[\pm \int_{\theta_-}^{\theta} \frac{\tilde{\gamma} \tilde{t}}{\sqrt{\Theta}} d\theta' \right]. \quad (3.46)$$

To interpret this equation, we will assume that the orbit is sufficiently close to r_0 that the change in r over the course of a period of motion in θ is negligible. Under this assumption (and with the fact that $d\lambda = d\theta/\sqrt{\Theta}$) we can write the integral in the exponent in Eq. (3.46) as

$$\int_{\theta_-}^{\theta} \frac{\tilde{\gamma} \tilde{t}}{\sqrt{\Theta}} d\theta' = \gamma \left[t(\theta) - t(\theta_-) \right] - \left(\frac{\Delta t}{\Delta \lambda} \right) [\lambda(\theta) - \lambda(\theta_-)], \quad (3.47)$$

where $\Delta t/\Delta \lambda$ is the average of $dt/d\lambda$ over a cycle of θ motion. We obtain this expression by using the fact that $dt/d\lambda$ is equivalent to \tilde{t} plus a constant when r (and hence \tilde{t}) does not change. Because \tilde{t} has zero average (by definition) over a period of θ motion, then when written in the form above, the constant must be $(\Delta t)/(\Delta \lambda)$. We can write this average rate of change in a useful form by noting that, from Eq. (3.13a) and Eqs. (3.11b),

$$\frac{dt}{d\lambda} = \frac{1}{2\Delta} \frac{\partial \mathcal{R}}{\partial \mathcal{E}} + a^2 \mathcal{E} \cos^2 \theta. \quad (3.48)$$

Averaging this expression over a cycle of θ motion, noting that the first term on the right-hand side is independent of θ , and using Eq. (3.11b) gives

$$\begin{aligned} \frac{\Delta t}{\Delta \lambda} &= \frac{1}{2\Delta} \frac{\partial \mathcal{R}}{\partial \mathcal{E}} + a^2 \mathcal{E} \left(\int_{\theta_-}^{\theta_+} \frac{\cos^2 \theta}{\sqrt{\Theta}} d\theta \right) \left(\int_{\theta_-}^{\theta_+} \frac{d\theta}{\sqrt{\Theta}} \right)^{-1} \\ &= \frac{1}{2\Delta} \frac{\partial \mathcal{R}}{\partial \mathcal{E}} + \frac{\partial \Delta S_{\theta} / \partial \mathcal{E}}{2\partial \Delta S_{\theta} / \partial \mathcal{Q}} \\ &= \frac{1}{2\Delta} \frac{\partial \mathcal{R}}{\partial \mathcal{E}} - \frac{1}{2} \left(\frac{d\mathcal{Q}}{d\mathcal{E}} \right)_{\text{BS}}. \end{aligned} \quad (3.49)$$

In the last step we have used the Bohr-Sommerfeld condition (3.41). Also according to Eq. (3.13a) and Eq. (3.13c), we can

find

$$t(\theta) - t(\theta_-) = \frac{\partial}{\partial \mathcal{E}} \int_{\theta_-}^{\theta} \sqrt{\Theta(\theta')} d\theta' + \frac{1}{2\Delta} \frac{\partial \mathcal{R}}{\partial \mathcal{E}} (\lambda(\theta) - \lambda(\theta_-)), \quad (3.50a)$$

$$\lambda(\theta) - \lambda(\theta_-) = 2 \frac{\partial}{\partial \mathcal{Q}} \int_{\theta_-}^{\theta} \sqrt{\Theta(\theta')} d\theta', \quad (3.50b)$$

where to derive these two equations, we can again use the fact that $d\lambda = d\theta/\sqrt{\Theta}$ and the definition of Θ ; for the first we also make use of Eq. (3.48).

Finally, we insert Eqs. (3.50a), (3.50b), and (3.49) into Eq. (3.47) to find

$$\int_{\theta_-}^{\theta} \frac{\tilde{\gamma} \tilde{t}}{\sqrt{\Theta}} d\theta' = (-i\gamma) \left[\frac{\partial}{\partial \mathcal{E}} + \left(\frac{d\mathcal{Q}}{d\mathcal{E}} \right)_{\text{BS}} \frac{\partial}{\partial \mathcal{Q}} \right] [iS_{\theta}(\theta)]. \quad (3.51)$$

Substituting Eq. (3.51) into the solution for A_{θ}^{\pm} in Eq. (3.46) gives that

$$A_{\theta}^{\pm} = \frac{\exp \left\{ (\pm i\gamma) \left[\frac{\partial}{\partial \mathcal{E}} + \left(\frac{d\mathcal{Q}}{d\mathcal{E}} \right)_{\text{BS}} \frac{\partial}{\partial \mathcal{Q}} \right] [iS_{\theta}(\theta)] \right\}}{\sqrt{\sin \theta \sqrt{\Theta}}}. \quad (3.52)$$

The phase in this equation, however, is precisely the correction to the leading-order expression for the phase $e^{iS_{\theta}(\theta)}$ if we allow \mathcal{E} and \mathcal{Q} to be complex, where their imaginary parts are given by

$$\text{Im} \mathcal{E} = -\gamma = -\omega_I, \quad \text{Im} \mathcal{Q} = \left(\frac{d\mathcal{Q}}{d\mathcal{E}} \right)_{\text{BS}} (-\gamma). \quad (3.53)$$

Through next-to-leading order, therefore, the θ portion of the wave is given by

$$A_{\theta}^+ e^{iS_{\theta}(\theta)} + A_{\theta}^- e^{-iS_{\theta}(\theta)} = \frac{e^{iS_{\theta}(\theta)} + e^{-iS_{\theta}(\theta)}}{\sqrt{\sin \theta \sqrt{\Theta}}}, \quad (3.54)$$

where \mathcal{E} and \mathcal{Q} used in S_{θ} are complex.

In the geometric-optics approximation, therefore, we have shown that we can account for the amplitude corrections to the wave by allowing the conserved quantities, \mathcal{E} and \mathcal{Q} , to be complex [with their imaginary parts given in Eq. (3.53)]. Furthermore, through the geometric-optics correspondence, and the definition of A_{lm}^I in Eq. (2.27) we can confirm that $A_{lm}^I = \mathcal{Q}_I$; therefore, the relationship

$$\mathcal{Q} = A_{lm} - m^2, \quad (3.55)$$

is true for a complex \mathcal{Q} and A_{lm} .

In closing, we note that at the same θ , the magnitude of the two components of the wave in Eq. (3.52) are not equal. More specifically, the integral involving \tilde{t} makes A^+ have a larger amplitude at $\theta < \pi/2$ and a smaller amplitude at $\theta > \pi/2$; A^- has the opposite profile. Therefore, the net wave function remains symmetric about $\theta = \pi/2$.

IV. FEATURES OF THE SPECTRA OF KERR BLACK HOLES

In this section, we will use the WKB formula and the geometric-optics correspondence in the first two sections of this paper to explain several aspects of the quasinormal-mode spectrum of Kerr black holes. Specifically, we will explain the absence of damping for a significant fraction of modes of extremal Kerr holes. We will also decompose the frequency into orbital and precessional parts and explain a degeneracy in the spectra of Kerr holes in terms of a rational relation of these frequencies when the corresponding photon orbits close.

A. Spherical photon orbits and extremal Kerr black holes

We will first review the properties of spherical photon orbits. These orbits can be found by setting $\mathcal{R}(r) = \mathcal{R}'(r) = 0$ (see, e.g., [34]), and their conserved quantities are fixed by the radius of the orbit r and the spin of the black hole a to be

$$\mathcal{Q}/\mathcal{E}^2 = -\frac{r^3(r^3 - 6Mr^2 + 9M^2r - 4a^2M)}{a^2(r-M)^2}, \quad (4.1a)$$

$$L_z/\mathcal{E} = -\frac{r^3 - 3Mr^2 + a^2r + a^2M}{a(r-M)}. \quad (4.1b)$$

We will next discuss additional features of these orbits.

For a given spin parameter a , there is a unique spherical photon orbit with parameters $(\mathcal{E}, L_z, \mathcal{Q})$ for any radius between the outermost and innermost photon orbits (the retrograde and prograde equatorial photon orbits). Their radii (which we denote r_1 for retrograde and r_2 for prograde orbits) are given by

$$r_1 = 2M \left[1 + \cos \left(\frac{2}{3} \arccos \left(-\frac{|a|}{M} \right) \right) \right], \quad (4.2a)$$

$$r_2 = 2M \left[1 + \cos \left(\frac{2}{3} \arccos \left(\frac{|a|}{M} \right) \right) \right]. \quad (4.2b)$$

At each $r_1 \leq r \leq r_2$, the spherical orbit's inclination angle reaches a maximum and minimum of θ_{\pm} (at which $\Theta = 0$). These angles are given by

$$\cos^2 \theta_{\pm} = \frac{\left[2\sqrt{M\Delta(2r^3 - 3Mr^2 + Ma^2)} - (r^3 - 3M^2r + 2Ma^2) \right] r}{a^2(r-M)^2}, \quad (4.3)$$

which are equivalent to the turning points of the integral (2.14) (and, therefore, we use the same symbols for these angles).

Using the geometric-optics correspondence between $(\mathcal{E}, L_z, \mathcal{Q})$ and $(\Omega_R, \mu, \alpha_{lm}^R)$, we see that equatorial orbits at r_1 and r_2 corresponds to modes with $\mu = -1$ and $+1$, respectively, or modes with $m = \pm l$ and $l \gg 1$ (strictly speaking, though, $\mu = m/(l+1/2)$ never precisely reaches ± 1). We can also relate r_p , the real root of Eq. (2.37), to the polar orbit and modes with $m = 0$. For orbits between

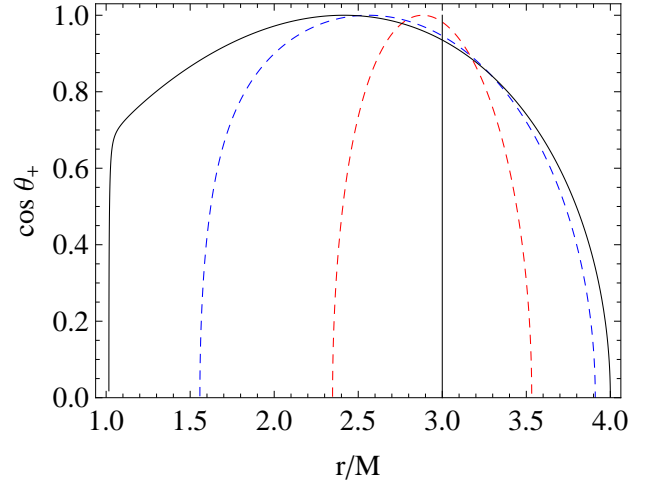


Figure 11: The values of r and $\cos \theta_+$ of spherical photon orbits, for $a/M = 0$ (black, solid vertical line), 0.5 [red (light gray) dashed curve], 0.9 [blue (dark gray) dashed curve] and 0.99999 (black, solid curve). Note that for $a = 0$, all such orbits have $r = 3M$, while for $a = M$, a significant fraction reside at $r = M$.

the equatorial and polar ones, we can use Eqs. (2.33a) and (2.33b) to obtain a μ between -1 and $+1$. Then, only those modes that can be written as $m/(l+1/2)$ with the allowed integer values of l and m correspond to a QNM (though the photon orbits that correspond to QNMs are a dense subset of all photon orbits).

Note in Fig. 11 that for $a \sim M$, a significant fraction of spherical photon orbits of different inclination angles all have nearly the same radius, $r \approx M$. Through the geometric-optics correspondence, a large fraction of modes (a finite range of values of μ) relate to this set of modes with $r \approx M$. In Fig. 12, we explicitly show the relation between modes characterized by μ and their corresponding spherical-photon-orbit radii (normalized by the horizon radius) for several values of a/M slightly less than unity. The radius exhibits an interesting transition between two kinds of behaviors: for $\mu > \mu_* \approx 0.744$, the value of r is very close to M (the horizon radius for an extremal Kerr black hole), and for $\mu < \mu_*$ the radii increase linearly. The orbits with $\mu > \mu_*$ have a range of inclination angles. Their $\sin \theta_{\pm}$ span from 0.731 (at μ_* , the most inclined orbit) to 1 (at $\mu = 1$, the prograde equatorial orbit).

For the extremal black holes, therefore, a nonzero fraction of corotating spherical photon orbits appear to coincide with the horizon in the Boyer-Lindquist coordinate system. Although the proper distance between these orbits will not vanish (see [36]), this does not seem to be a coordinate effect, because there is a definite physical change of the modes for these values of $\mu > \mu_*$. By comparing with Fig. 12 with Fig. 5, we see that these orbits also have $\Omega_l \approx 0$. A vanishing imaginary part of the frequency corresponds to a vanishing of the radial Lyapunov exponent for this entire nonzero region of spherical photon orbits. This, therefore, would lead to a curious effect for a highly spinning black hole: for perturbations with $\mu \geq \mu_*$, modes do not move away from or into the horizon very quickly. If we were to solve an initial-data problem con-

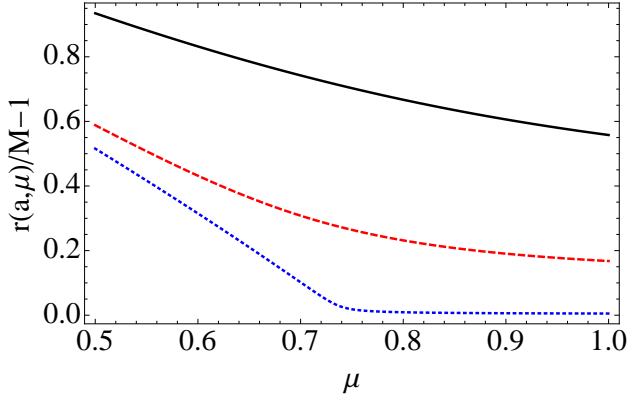


Figure 12: Radii of corotating spherical photon orbits as a function of μ , for $a/M = 0.9$ (black solid line), 0.99 (red dashed curve), 0.9999 (blue dotted line). For extremal Kerr black holes, a nonzero fraction of all spherical photon orbits are on the horizon.

taining these modes, we would find that they live for a long time; moreover, because these are nearly equatorial modes, we would see that the final, long-lived perturbations escape in the equatorial direction. This would imply that if we were to drive the black hole appropriately with equatorial incoming radiation, we would excite these nearly lossless modes with high amplitude (like optically exciting a resonant cavity with high finesse).

B. A mode's orbital and precessional frequencies

In this part, we will define two frequencies associated with individual spherical photon orbits (the orbital and precessional frequencies) and understand their connection to the real part of the QNM frequency. We begin by noting that because spherical photon orbits have only two independent degrees of freedom describing their motion [see, e.g., Eq. (4.1)], the orbit can be characterized by two frequencies. The first is the θ -frequency, Ω_θ , the frequency at which the particle oscillates below and above the equatorial plane. During each θ -cycle, which takes an amount of time given by $T_\theta = 2\pi/\Omega_\theta$, the particle also moves in the azimuthal (or ϕ) direction. If this angle is 2π for a corotating orbit ($m > 0$) or -2π for a counterrotating orbit ($m < 0$), then there is no precession (and these simple, closed orbits have effectively one frequency describing their motion, as the spherical photon orbits of a Schwarzschild black hole do). The difference between the $\Delta\phi$ and $\pm 2\pi$ (its precession-free value) we will denote as the *precession angle*,

$$\Delta\phi_{\text{prec}} \equiv \Delta\phi - 2\pi \text{sgn } m, \quad (4.4)$$

where $\text{sgn } m$ is the sign of m . We can also associate the rate of change of ϕ_{prec} with a frequency,

$$\Omega_{\text{prec}} \equiv \Delta\phi_{\text{prec}}/T_\theta = \Delta\phi_{\text{prec}}\Omega_\theta/(2\pi). \quad (4.5)$$

Both T_θ and $\Delta\phi_{\text{prec}}$ can be computed from geodesic motion [see the formulas for Ω_θ and $\Delta\phi_{\text{prec}}$ in Eq. (4.8)].

It is possible to perform split of the real part of the QNM into two analogous frequencies. To derive this split, start from a single ray, along which the phase of the wave must be constant. Also suppose that the ray originates from θ_- and ends at θ_+ after traveling only one-half of a cycle of motion in the θ direction. During this time, the statement that the phase is unchanged is that

$$0 = -\omega_R T_\theta/2 + (L - |m|)\pi + m\Delta\phi/2. \quad (4.6)$$

Using (half of) Eq. (4.4), the real part of the frequency is

$$\omega_R = L\Omega_\theta(m/L) + m\Omega_{\text{prec}}(m/L). \quad (4.7)$$

Note that Ω_θ and Ω_{prec} both depend on m/L .

More explicitly, given the orbital parameters $(\mathcal{E}, \mathcal{Q}, L_z)$, the quantities T_θ and $\Delta\phi$ can be obtained by computing

$$T_\theta = \frac{\partial}{\partial \mathcal{E}} \oint \sqrt{\Theta} d\theta + \frac{1}{2\Delta} \frac{\partial \mathcal{R}}{\partial \mathcal{E}} \oint \frac{d\theta}{\sqrt{\Theta}}, \quad (4.8a)$$

$$\Delta\phi = -\frac{1}{L_z} \left[1 - \frac{\partial}{\partial \log \mathcal{E}} \right] \oint \sqrt{\Theta} d\theta + \frac{1}{2\Delta} \frac{\partial \mathcal{R}}{\partial L_z} \oint \frac{d\theta}{\sqrt{\Theta}}, \quad (4.8b)$$

(expressions that hold for any spherical photon orbit—*not* simply orbits that satisfy the Bohr-Sommerfeld condition) and the two frequencies are given by

$$\Omega_\theta = 2\pi \left(\frac{\partial}{\partial \mathcal{E}} \oint \sqrt{\Theta} d\theta + \frac{1}{2\Delta} \frac{\partial \mathcal{R}}{\partial \mathcal{E}} \oint \frac{d\theta}{\sqrt{\Theta}} \right)^{-1} \quad (4.9a)$$

$$\Omega_{\text{prec}} = \Omega_\theta \frac{\Delta\phi}{2\pi} - (\text{sgn } L_z)\Omega_\theta. \quad (4.9b)$$

These can be expressed in terms of $(\mathcal{E}, \mathcal{Q}, L_z)$ using elliptic integrals (as was done in [37]), but we will not carry this out explicitly.

For very slowly spinning black holes, a short calculation shows that

$$\Omega_\theta \approx \frac{1}{\sqrt{27M}} = \sqrt{\frac{M}{r_0^3}}, \quad (4.10a)$$

$$\Omega_{\text{prec}} \approx \frac{2a}{27M^2} = \frac{2S}{r_0^3}, \quad (4.10b)$$

where r_0 is the circular-photon-orbit radius for a Schwarzschild black hole, $r_0 = 3M$, and $S = aM$. The expression for Ω_θ is the Keplerian frequency of the spherical photon orbit, and $\Omega_{\text{prec}} = 2S/r_0^3$ is the Lense-Thirring precessional frequency. In the slow-rotation limit, therefore, our formula recovers Ferrari and Mashhoon's result [9].

For any value of a , we can normalize Eq. (4.7) by L , and write

$$\Omega_R(a, \mu) = \Omega_\theta(a, \mu) + \mu\Omega_{\text{prec}}(a, \mu). \quad (4.11)$$

In Figs. 13 and 14, we explore the two frequencies in the decomposition of Ω_R by separately plotting Ω_θ and Ω_{prec} , for different values of a .

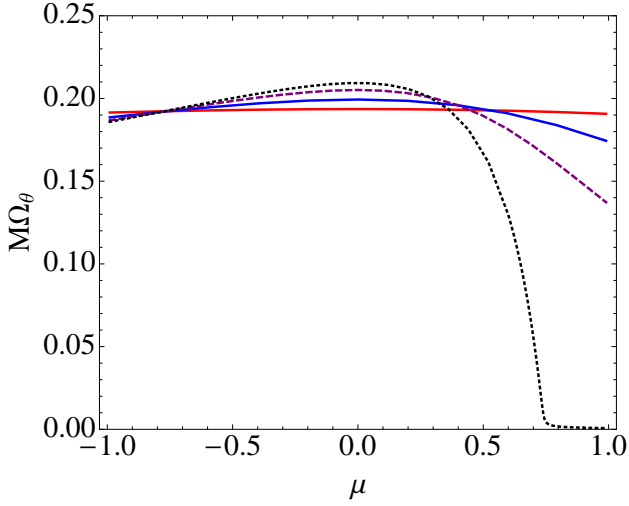


Figure 13: Orbital frequency, Ω_θ , plotted against μ , for $a/M = 0.3$ [red (light gray) solid curve], 0.7 [blue (dark gray) solid curve], 0.9 (purple dashed line), and 1 (black dotted line). The orbital frequency vanishes for a significant range of μ for extremal black holes.

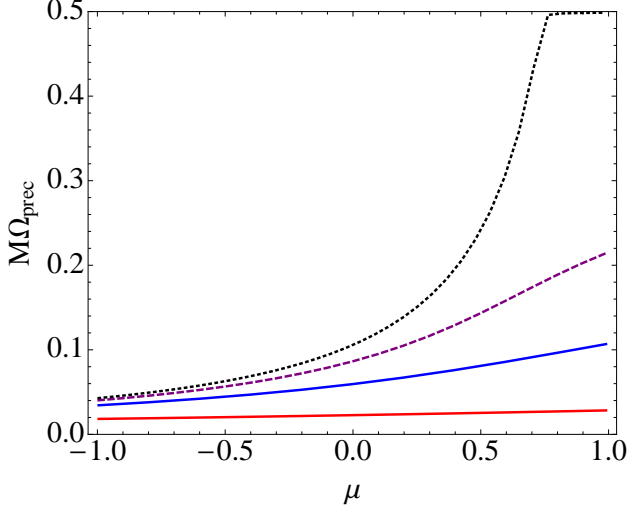


Figure 14: Precessional frequency, Ω_ϕ , versus μ plotted identically to those curves in Fig. 13 representing the same black-hole spins. The precessional frequency approaches the horizon frequency, Ω_H , for a range of values of μ for extremal black holes.

For small values of a/M , Ω_θ and Ω_{prec} are consistent with the constant values predicted by Eqs. (4.10a) and (4.10b). For larger values of a/M , Ω_θ does not vary much as a function of μ until $a \sim 0.7M$; for spins greater than this value, it is only for larger values of μ that Ω_θ changes significantly by decreasing from the equivalent values for $a = 0$. Finally, as $a \rightarrow M$, Ω_θ vanishes for $\mu \geq \mu_* \approx 0.744$. The precessional frequency, Ω_{prec} , on the other hand, monotonically increases as a function of μ even for small values of a/M ; as $a \rightarrow M$, Ω_{prec} grows to Ω_H at $\mu \sim \mu_*$, and stays there for all values of $\mu > \mu_*$. For $a \sim M$ and $\mu > \mu_*$, there is one additional feature worth noting: because $\Omega_\theta \sim 0$ and $\Omega_\phi \sim \Omega_H$, this gives rise to the interpretation of the mode as a ray that sticks on the

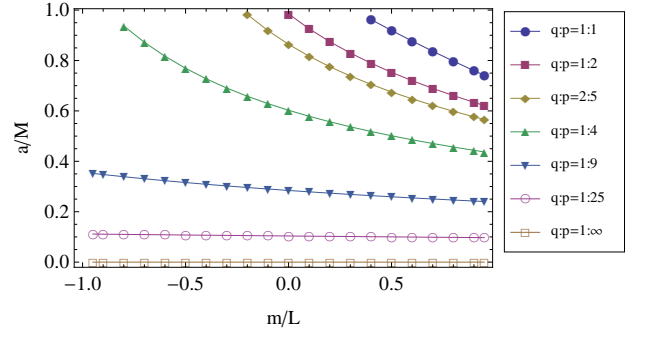


Figure 15: A diagram showing the spin parameters, a , and the ratios of the multipolar indexes m/L , at which the orbital and precessional frequencies have a ratio of p/q . Although we only perform our numerical calculations at a discrete set of m/L values (shown by the dots), in the eikonal limit, each set of points for a given ratio of p/q approaches a continuous curve.

horizon and corotates with the horizon at its angular frequency of Ω_H ; moreover, there seems to be no restoring force along the θ direction.

C. Degenerate quasinormal modes and closed spherical photon orbits

Finally, in this section, we interpret the degeneracy of QNM frequencies (of which Fig. 1 was an example). Recall that in that figure, for $a/M \approx 0.7$, we found pairs of modes such as $(2, 2)$ and $(3, -2)$, $(3, 2)$ and $(4, -2)$, $(4, 2)$ and $(5, -2)$, and so on, all have approximately the same frequency. For another, lower spin $a/M \approx 0.4$, pairs like $(3, 3)$ and $(4, -3)$, $(4, 3)$ and $(5, -3)$, et cetera, have approximately the same frequency.

The approximate degeneracy exists because the ratio between Ω_θ and Ω_{prec} can be rational, and the photon orbits close. If for a certain mode of a black hole with spin a , with m and L , and for integers p and q ,

$$q\Omega_\theta \left(a, \frac{m}{L} \right) = p\Omega_{\text{prec}} \left(a, \frac{m}{L} \right), \quad (4.12)$$

this means that there exists a closed spherical photon orbit that satisfies the conditions necessary to correspond to a QNM. Equation (4.12) implies that

$$\begin{aligned} & L\Omega_\theta \left(a, \frac{m}{L} \right) + m\Omega_{\text{prec}} \left(a, \frac{m}{L} \right) \\ & = (L + kq)\Omega_\theta \left(a, \frac{m}{L} \right) + (m - kp)\Omega_{\text{prec}} \left(a, \frac{m}{L} \right). \end{aligned} \quad (4.13)$$

If Ω_θ and Ω_{prec} do not change much from $\mu = m/L$ to $\mu' = (m - kp)/(L + kq)$ (either because spin is small—and therefore Ω_θ and Ω_{prec} depend weakly on μ —or because $L \gg kq$ and $m \gg kp$), then

$$\omega_R^{l,m} \approx \omega_R^{l+kq, m-kp}. \quad (4.14)$$

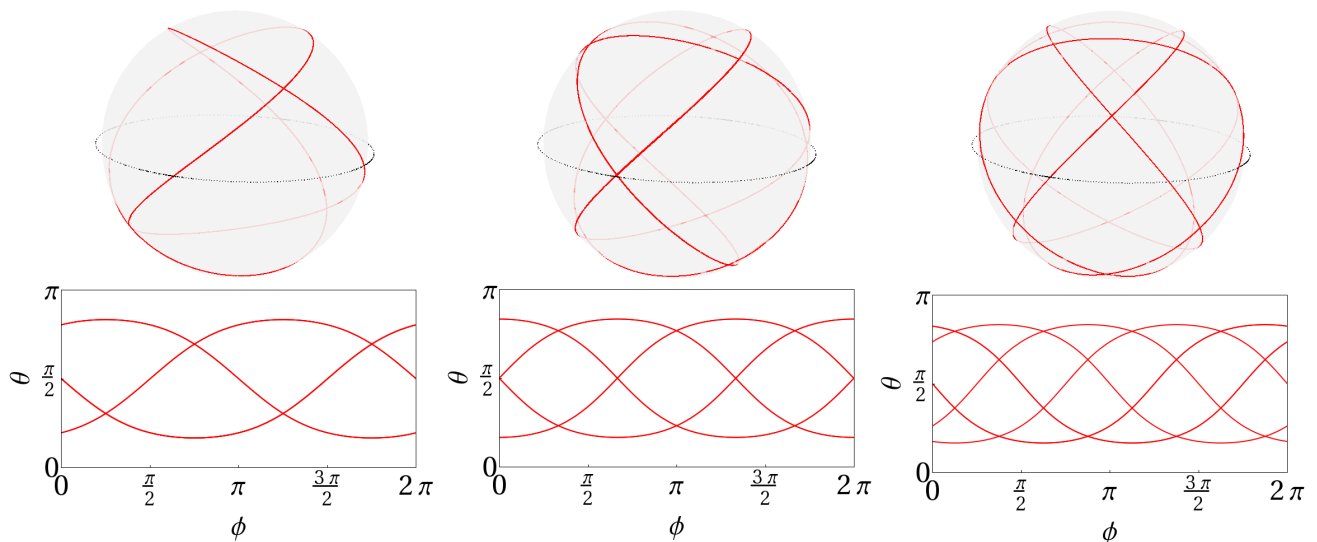


Figure 16: For black holes with spins $a/M = 0.768, 0.612,$ and 0.502 , the spherical photon orbits with $\omega_{\text{orb}} = 2\omega_{\text{prec}}$, on the left, $\omega_{\text{orb}} = 3\omega_{\text{prec}}$ in the center, and $\omega_{\text{orb}} = 4\omega_{\text{prec}}$ on the right, respectively. These orbits correspond to quasinormal modes in the eikonal limit with $m/L = 0.5$. The top figures show the photon orbit, the red, solid curve, on its photon sphere (represented by a transparent sphere). The dashed black line is the equatorial ($\theta = \pi/2$) plane, which was inserted for reference. The bottom figures are the same photon orbits, but plotted in the ϕ - θ plane, instead.

Because Ω_l depends similarly on μ , under the same conditions,

$$\omega_l^{l,m} \approx \omega_l^{l+kq, m-kp}; \quad (4.15)$$

therefore, the modes are degenerate. It is also clear from Eq. (4.12) that the degeneracy happens at the same time that the corresponding orbit is closed. The three series mentioned at the beginning of the paper correspond to $p/q = 4, 6,$ and 8 , respectively (for $k = 1$).

1. Slowly spinning black holes

For $a/M \ll 1$, when Eqs. (4.10a) and (4.10b) apply, the condition for degenerate modes becomes

$$\frac{q\sqrt{27}}{2p} = \frac{a}{M} \ll 1 \quad (4.16)$$

(a statement that holds independent of μ). This implies that orbits of all inclinations close for these spins.

For these specific spins, the QNM spectrum is completely degenerate, by which we mean that all modes have the same decay rate, and all real parts of the frequencies are integer multiples of only one frequency (similar to those of a Schwarzschild black hole). Using this approximate formula to find a for the three instances of degeneracy in Fig. 1, we find

$$a_{4/1} \approx 0.65M, \quad a_{6/1} \approx 0.43M, \quad a_{8/1} \approx 0.32M. \quad (4.17)$$

These are not very far away from spins we found empirically.

2. Generic black holes

For a generic spin parameter a , we will explain degeneracies that exist around a mode with $L \gg 1$ and $|m| \gg 1$. If the condition in Eq. (4.12) holds for $p, q \ll \min(L, |m|)$, then there is a range of $|k| \ll \min(L, |m|)/\max(p, q)$ in which there is a degeneracy between all $(L+kq, m-kp)$ and (L, m) . These modes must be those close to the mode of indices (L, m) , because, strictly speaking, it is only the orbit corresponding to m/L which is precisely closed.

To find this degeneracy, we will search for spin parameters a for which Eq. (4.12) holds for any set of indexes (L, m) and integers (p, q) that satisfy $L, |m| \gg p, q$ (we generally either find one or zero solutions). To visualize this degeneracy, for each pair (p, q) , we will mark all possible pairs of $(m/L, a)$ in a 2D plot; the values of the spins are sufficiently dense for each value of m/L that they form a smooth curve when plotted against m/L . Some of these curves are shown in Fig. 15. Because for a fixed p/q the degenerate spins for $a/M \lesssim 0.3$ are nearly independent of m/L , Eq. (4.16) should be an accurate prediction for spins less than that value. As a concrete illustration of the orbits corresponding to these degenerate modes, we plot closed orbits for $m/L = 0.5$ and for $a/M \approx 0.5, 0.61,$ and 0.77 in Fig. 16. The values of the spins agree quite well with those predicted in Fig. 15.

V. CONCLUSIONS AND DISCUSSION

In this paper, we extended the results of several earlier works [9, 27, 31, 32] to compute the quasinormal-mode frequencies and wave functions of a Kerr black hole of arbitrary

astrophysical spins, in the eikonal limit ($l \gg 1$). We focused on developing a greater intuitive understanding of their behavior, but, in the process, we calculated expressions for large- l quasinormal-mode frequencies that are reasonably accurate even at low l . Specifically, we applied a WKB analysis to the system of equations defined by the angular and radial Teukolsky equations. Using a Bohr-Sommerfeld condition for the angular equation, we related the angular separation constant to the frequency; when we expanded the constraint to leading order in $a\omega/l$, we found an equally accurate and algebraically simpler relation between the frequency and angular eigenvalue. We then used a well-known WKB analysis on the radial Teukolsky equation to obtain expressions for the QNM frequencies and the angular separation constants. The accuracy of the approximate expressions for the QNM frequency are observed to be of order $O(L^{-2})$ even though we had only expected a $O(L^{-1})$ convergence for the imaginary part.

Next, we reviewed that a massless scalar wave in the leading-order, geometric-optics approximation obeys the Hamilton-Jacobi equations, which are very similar to the Teukolsky equations when $l \gg 1$. By identifying terms in the Hamilton-Jacobi equations and Teukolsky equations, we related the conserved quantities of the Hamilton-Jacobi equations to the eigenvalues of the separated Teukolsky equations. Specifically, we confirmed that the energy, angular momentum in the z direction, and Carter constant in the Hamilton-Jacobi equations correspond to the real frequency, the index m , and the angular eigenvalue minus m^2 in the Teukolsky equations, respectively. Furthermore, we found that the conditions that define a quasinormal mode in the WKB approximation are equivalent to the conditions in the geometric-optics approximation that determine a spherical photon orbit that satisfies an identical Bohr-Sommerfeld quantization condition.

By analyzing the next-to-leading-order, geometric-optics approximation, we showed that the corrections to the amplitude of the scalar wave correspond to the imaginary parts of the WKB quantities. Specifically, we saw that the imaginary part of the frequency is equal to a positive half-integer times the Lyapunov exponent averaged over a period of motion in the θ direction. The imaginary part of the angular eigenvalue is equal to the imaginary part of the Carter constant, which is, in turn, related to an amplitude correction to geometric-optics approximation to the angular function for θ .

We then applied these results to study properties of the QNM spectra of Kerr black holes. We observed that for extremal Kerr black holes a significant fraction of the QNMs have nearly zero imaginary part (vanishing damping) and their corresponding spherical photon orbits are stuck on the horizon (in Boyer-Lindquist coordinates). We plan to study this unusual feature of extremal Kerr black holes in future work. In addition, we showed that for Kerr black holes of any spin, the modes' frequencies (in the eikonal limit) are a linear combination of the orbital and precession frequencies of the corresponding spherical photon orbits. This allows us to study an intriguing feature of the QNM spectrum: namely, when the orbital and precession frequencies are rationally related—i.e., when the spherical photon orbits are closed—then the corresponding quasinormal-mode frequencies are also degenerate.

We hope that the approximate expressions for the quasinormal-mode frequencies in this paper will prove helpful for understanding wave propagation in the Kerr spacetime. This not unreasonable to suppose, because Dolan and Ottewill have shown in [26, 28] that to calculate the Green's function analytically in the Schwarzschild spacetime, one needs to know analytical expressions for the frequency of the quasinormal modes (specifically, this comes from the fact that the frequencies of the quasinormal mode are the poles of the Green's function in the frequency domain). We, therefore, think that our approximate formulas could assist with the calculation of the Green's function in the Kerr spacetime, in future work.

Acknowledgments

We thank Emanuele Berti for discussing this work with us and pointing out several references to us. We also thank Jeandrew Brink for insightful discussions about spherical photon orbits in the Kerr spacetime. We base our numerical calculation of the QNM frequencies on the Mathematica notebook provided by Emanuele Berti and Vitor Cardoso [38]. This research is funded by NSF Grants PHY-1068881, PHY-1005655, CAREER Grant PHY-0956189; NASA Grant No.NNX09AF97G; the Sherman Fairchild Foundation, the Brinson Foundation, and the David and Barbara Groce Startup Fund at Caltech.

Appendix A: The Taylor expanded Bohr-Sommerfeld condition

The Bohr-Sommerfeld constraint (2.14) gives us a way to evaluate A_{lm} in terms of l , m , and ω ; the error in this approximation scales as $1/l$. Because it is an integral equation, it is not particularly convenient to solve, and it is beneficial to have an approximate, but algebraic expression for the frequency of a QNM. With the benefit of hindsight, one can confirm through numerical calculations of exact QNM frequencies performed using Leaver's method that the parameter $a\omega/l$ is numerically a small number for all black hole spins. We can then expand the angular separation constant, A_{lm} , in a series in $a\omega/l$ as $A_{lm} = A_{lm}^0 + \delta A_{lm}$, where A_{lm}^0 satisfies the equation

$$\int_{\theta_-^0}^{\theta_+^0} \sqrt{A_{lm}^0 - \frac{m^2}{\sin^2 \theta}} = \pi \left(l + \frac{1}{2} - |m| \right), \quad (\text{A1})$$

and at leading order, $\theta_+^0, \theta_-^0 = \pm \arcsin[m/(l+1/2)]$. One can easily verify that the solution to this equation is the angular eigenvalue of a Schwarzschild black hole, $A_{lm}^0 = (l+1/2)^2$ (note that we are assuming $l \gg 1$). Now we will compute the lowest-order perturbation in $a\omega/l$, which turns out to be quadratic in this parameter [i.e., $(a\omega/l)^2$] below:

$$\int_{\theta_-^0}^{\theta_+^0} \frac{\delta A_{lm} + a^2 \omega^2 \cos^2 \theta}{\sqrt{(l+1/2)^2 - m^2/\sin^2 \theta}} d\theta = 0. \quad (\text{A2})$$

The integration limits θ_+, θ_- also can be expanded in a series in $a\omega/l$, and the lowest-order terms of this series are given by θ_+^0, θ_-^0 ; The perturbation in θ_+, θ_- would result in some quartic corrections in $a\omega/l$ [i.e., $(a\omega/l)^4$] when we evaluate the integrals of Eqs. (A2) and (A1), because the integrand is of order $(a\omega/l)^2$ and the width of the correction in θ_+, θ_- are also of order $(a\omega/l)^2$. As a result, we will not need it here. Evaluating the integral in Eq. (A2) is straightforward, and we find

$$A_{lm} = A_{lm}^0 + \delta A_{lm} = l(l+1) - \frac{a^2\omega^2}{2} \left[1 - \frac{m^2}{l(l+1)} \right] \quad (\text{A3})$$

Interestingly, the above expression is consistent with the expansion of A_{lm} for small $a\omega$ given in [39], even in the eikonal

limit, where $a\omega$ is large. The reason for this fortuitous agreement is again that for QNMs of Kerr black holes of any spin, $a\omega/l$ is small, and the expansion only involves even powers of this parameter, $(a\omega/l)^2$. Because the coefficients in the expansion of $a\omega$ scale as $1/l^k$ for even powers of $(a\omega)^k$ and $1/l^{k+1}$ for odd powers of $(a\omega)^k$, in the limit of large l , the two series actually are equivalent in the eikonal limit. In principle, one can also expand and solve Eq. (2.14) to higher orders in the parameter $a\omega/l$ and compare with the expansion in $a\omega$ in [39]; we expect that the two series should agree. This would be useful, because it would effectively let one use the small $a\omega$ expansion in the eikonal limit, where the series would, ostensibly, not be valid.

-
- [1] C. V. Vishveshwara, *Nature* **227**, 936 (1970).
[2] K. D. Kokkotas and B. Schmidt, *Living Rev. Relativity* **2**, 2 (1999), <http://www.livingreviews.org/lrr-1999-2>.
[3] H.-P. Nollert, *Classical Quantum Gravity* **16**, R159 (1999).
[4] V. Ferrari and L. Gualtieri, *Gen. Relativ. Gravit.* **40**, 945 (2008).
[5] E. Berti, V. Cardoso, A. O. Starinets, *Classical Quantum Gravity* **26**, 163001 (2009).
[6] R. A. Konoplya and A. Zhidenko, *Rev. Mod. Phys.* **83**, 793 (2011).
[7] M. Davis, R. Ruffini, W. H. Press, and R. H. Price, *Phys. Rev. Lett.* **27**, 1466 (1971).
[8] S. Chandrasekhar and S. Detweiler, *Proc. R. Soc. Lond. A* **344**, 441 (1975).
[9] V. Ferrari and B. Mashhoon, *Phys. Rev. D* **30**, 295 (1984).
[10] B. F. Schutz and C. M. Will, *Astrophys. J.* **291**, L33 (1985).
[11] S. Iyer and C. M. Will, *Phys. Rev. D* **35**, 3621 (1987).
[12] E. W. Leaver, *Proc. R. Soc. Lond. A* **402**, 285 (1985).
[13] H.-P. Nollert, *Phys. Rev. D* **47**, 5253 (1993).
[14] E. W. Leaver, *Phys. Rev. D* **34**, 384 (1986).
[15] Y. Sun and R. H. Price, *Phys. Rev. D* **38**, 1040 (1988).
[16] <http://www.ligo.caltech.edu/>
[17] <http://www.ego-gw.it/public/virgo/virgo.aspx>
[18] F. Echeverria, *Phys. Rev. D* **40**, 3194 (1989).
[19] E. E. Flanagan, and S. A. Hughes, *Phys. Rev. D* **57**, 4566 (1998).
[20] A. Buonanno, G. B. Cook, and F. Pretorius, *Phys. Rev. D* **75**, 124018 (2007).
[21] E. Berti, V. Cardoso, J. A. Gonzalez, U. Sperhake, M. Hannam, S. Husa, and B. Brügmann, *Phys. Rev. D* **76**, 064034 (2007).
[22] O. Dreyer, B. Kelly, B. Krishnan, L. S. Finn, D. Garrison, and R. Lopez-Aleman, *Classical Quantum Gravity* **21**, 787 (2004).
[23] E. Berti, V. Cardoso, and C. M. Will, *Phys. Rev. D* **73**, 064030 (2006).
[24] A. Zimmerman and Y. Chen, *Phys. Rev. D* **84**, 084012 (2011).
[25] Y. Mino and J. Brink, *Phys. Rev. D* **78**, 124015 (2008).
[26] S. R. Dolan and A. C. Ottewill, *Classical Quantum Gravity* **26**, 225003 (2009).
[27] S. R. Dolan, *Phys. Rev. D* **82**, 104003 (2010).
[28] S. R. Dolan and A. C. Ottewill, *Phys. Rev. D* **84**, 104002 (2011).
[29] V. Cardoso, A. S. Miransa, E. Berti, H. Witek, V. T. Zanchin, *Phys. Rev. D* **79**, 064016 (2009).
[30] S. A. Teukolsky, *Phys. Rev. Lett.* **29**, 1114 (1972).
[31] K. D. Kokkotas, *Classical Quantum Gravity* **8**, 2217 (1991).
[32] E. Seidel and S. Iyer, *Phys. Rev. D* **41**, 374 (1990).
[33] S. Detweiler, *Astrophys. J.* **239**, 292 (1980).
[34] S. Chandrasekhar, *The Mathematical Theory of Black Holes* (Oxford University Press, Oxford, 1983).
[35] C. W. Misner, K. S. Thorne and J. A. Wheeler, *Gravitation*, (W. H. Freeman and Company, New York, 1973).
[36] J. M. Bardeen, W. H. Press, and S. A. Teukolsky, *Astrophys. J.* **178**, 347 (1972).
[37] E. Teo, *Gen. Relativ. and Gravit.* **35**, 1909 (2003).
[38] <http://www.phy.olemiss.edu/berti/qnms.html>
[39] E. Berti, V. Cardoso, M. Casals, *Phys. Rev. D* **73**, 024013 (2006).